18 Ossabaw Island Miniature Swine: Metabolic Syndrome and Cardiovascular Assessment

Michael Sturek, Johnathan D. Tune, and Mouhamad Alloosh.
Sturek, M., J.D. Tune, and M. Alloosh. Ossabaw Island miniature swine: metabolic syndrome and cardiovascular assessment. In *Swine in the Laboratory: Surgery, Anesthesia, Imaging, and Experimental Techniques,* Third Edition. M.M. Swindle (Ed.). Boca Raton: CRC Press, (In press, 2015). [CD supplement includes 28 figures and 44 videos.]

INTRODUCTION

Ossabaw swine were deposited on Ossabaw Island, GA, in the 1500s by Spanish explorers (Mayer and Brisbin, Jr., 1991) and, since then, the ocean has remained an impenetrable barrier to emigration of Ossabaw pigs to the mainland. Natural models of disease that arise from adaptation of animals to unique selection pressures can give insights into similar complex, multifactorial diseases in humans. Ossabaw miniature swine may recapitulate the natural pathogenesis of type 2 diabetes because of their "thrifty genotype" that enabled survival in the feast and famine ecology of Ossabaw Island. The thrifty genotype hypothesis is that in the hunter-gatherer stages of human development the ability to store excess fat enabled survival during periods of famine (Neel, 1962).

In the 1970s and early 1980s, Ossabaw miniature swine were studied by ecologists for their unique adaptations in their natural habitat on Ossabaw Island (Mayer and Brisbin, Jr., 1991; Stribling et al., 1984) and, after establishment of colonies on the mainland, Ossabaws were studied by animal scientists for their propensity to obesity (Buhlinger et al., 1978; Martin et al., 1973; Martin and Herbein, 1976; Weiss et al., 1974), insulin resistance (Wangsness et al., 1977), plasma lipoproteins (Etherton and Kris-Etherton, 1980), and renal physiology (Zervanos et al., 1983).

Renewed interest in Ossabaw miniature swine was sparked in 2001 with the realization of the obesity and diabetes epidemic (Bellenger et al., 2006; Mokdad et al., 2001) and Brisbin's timely appeal to the scientific community to save feral Ossabaw Island swine from eradication by the Georgia Department of Natural Resources for environmental reasons (Brisbin and Mayer, 2001). Our laboratory obtained animals from the island in an expedition in 2002 and established a breeding colony at Indiana University. We have conducted studies involving obesity, metabolic syndrome, and diabetes and have made comparisons to the Yucatan miniature swine model (Boullion et al., 2003; Dixon et al., 1999, 2002; Edwards et al., 2006; Hainsworth et al., 2002; Kaser et al., 2004; Lloyd et al., 2006; Mokelke et al., 2003, 2005a, 2005b; Sheehy et al., 2006; Sturek et al., 2006; Witczak et al., 2004, 2005; Zafar et al., 2004).

The natural pathogenesis of type 2 diabetes involves a tendency to obesity with gradually increasing impairment of insulin action in a "prediabetes" condition, which has also been termed the *metabolic syndrome* or *cardiometabolic risk* (Eckel et al., 2005, 2006; Grundy et al., 2005; Kahn et al., 2005). In later stages, there is a significant increase in fasting blood glucose, which defines diabetes. Intensive research is under way to meet the need for animal models to understand

these comorbidities and develop therapies. The metabolic syndrome Ossabaw pig could be an outstanding large animal model. Strategies involving transgenic manipulations in other species and other breeds of minipigs are under development.

The metabolic syndrome in humans is actually a cluster of risk factors that includes (1) central (intra-abdominal) obesity, (2) insulin resistance, (3) impaired glucose tolerance, (4) dyslipidemia as measured by decreased plasma high-density lipoprotein (HDL) cholesterol compared to low-density lipoprotein (LDL), i.e., increased LDL/HDL ratio, (5) dyslipidemia as shown by increased plasma triglyceride, and (6) hypertension (Eckel et al., 2005; Ford et al., 2004; Grundy et al., 2004; McGill, Jr. et al., 2002). Although the definition and precise clinical utility have recently been controversial (Kahn et al., 2005), generally the presence of three of these characteristics renders a diagnosis of the cardiometabolic syndrome (Eckel et al., 2006; Grundy et al., 2004).

CHARACTERIZATION OF THE MODEL

The most critical question regarding the use of Ossabaw miniature swine was: Did removals from Ossabaw Island in 2002 have the thrifty genotype characteristics, i.e., "metabolic syndrome," found in the early characterization during ~1970–1985? Data collected to study these characteristics definitively confirm the early data, thus providing a rationale for more cardiovascular characterization, which was not performed in the early studies. The attached DVD includes experimental methods and images of metabolic syndrome (e.g. glucose tolerance) and cardiovascular characterization. The main criterion for the use of the Ossabaw miniature swine is the natural occurrence of metabolic syndrome and progression to type 2 diabetes with concomitant cardiovascular disease, which is unique to the Ossabaw. We further emphasize and highlight that the miniature size (~30 kg) of the Ossabaw at sexual maturity provides another advantage for husbandry and for study of sex differences in metabolic syndrome, type 2 diabetes, cardiovascular disease, etc. Although outstanding work shows that a line of crossbred domestic pigs with familial hypercholesterolemia will develop MetS (Bellinger et al., 2006), use of the standard sized domestic swine is not practical because they weigh >250 kg and are 2 years of age before metabolic syndrome occurs. Thus, in addition to the metabolic characteristics of Ossabaw miniature swine, the relatively small stature (30-80 kg) of Ossabaw pigs is essential (Dyson et al., 2006; Edwards et al., 2008; Langohr et al., 2008; Lloyd et al., 2008; Mattern et al., 2007).

Table 18.1 compares the major features of metabolic syndrome (items 1-6) present (Yes) or not (No) in Yucatan vs. Ossabaw miniature swine and their utility as cardiovascular disease models (item 7). The Yucatan is our comparison because of our extensive, ~25 years of work with this genetically leaner pig that is the predominantly used miniature swine for laboratory research; however, almost any other pig has characteristics of the Yucatan pig. We provide mainly the summary message here and leave detailed descriptions of our methods and experimental designs to the literature citations and the figures in the attached DVD. Ossabaws clearly show greater propensity to obesity than Yucatans and direct measures show a greater accumulation of visceral fat on rigorously controlled experimental diets. Despite intensive efforts to induce insulin resistance and glucose intolerance in Yucatan swine on high fat, high cholesterol, and high sucrose diets, we were not able to reproduce the findings of Phillips and colleagues were nearly 25 years ago (Panepinto et al., 1982; Phillips et al., 1982a; Phillips et al., 1982b). We emphasize that currently available lines of Yucatans do not naturally develop obesity-associated insulin resistance (Otis et al., 2003). In contrast, Ossabaw swine fed a high calorie diet display a natural pathogenesis of all metabolic syndrome characteristics. Other miniature swine breeds currently available for laboratory animal medicine, e.g. Yucatan and Gottingen, also do not progress to type 2 diabetes (e.g. Larsen et al., 2007; Otis et al., 2003; Phillips et al., 1982a). Gottingen pigs (Larsen et al., 2002; Larsen et al., 2005; Larsen et al., 2007; Larsen et al., 2006), however, will develop

mild metabolic syndrome. Published data and those on the DVD show that Ossabaw pigs with metabolic syndrome have vascular calcification and extreme coronary atheroma (Table 18.1, item 7), thus it is feasible to stent natural atherosclerotic lesions, not balloon-injured healthy arteries (e.g. Edwards et al., 2008; Gal and Isner, 1992; Johnson et al., 1999; Lowe et al., 2003; Schwartz and Edelman, 2002; Touchard and Schwartz, 2006).

TABLE 18.1
Comparison of metabolic syndrome (items 1-6) in Yucatan and Ossabaw miniature swine and utility as cardiovascular disease model (item 7)

Characteristic	Yucatan	Ossabaw	Reference
1. Obesity	No	Oss>Yuc	(Bell et al., 2010; Bender et al., 2009; Berwick et al., 2012; Berwick et al., 2013; Bonin et al., 2012; Boullion et al., 2003; Bratz et al., 2008; Clark et al., 2011; Dincer, 2011; Dyson et al., 2006; Edwards et al., 2010; Elmadhun et al., 2014a; Elmadhun et al., 2013; Faris et al., 2012; Flum et al., 2007; Hamamdzic and Wilensky2013; Handa et al., 2014a; Handa et al., 2014b; Handa et al., 2014c; Hanhineva et al., 2013; Kreutz et al., 2011; Lassaletta et al., 2012; Lee et al., 2009; Li et al., 2012; Li et al., 2011; McKenney et al., 2014; Moberly et al., 2013; Neeb et al., 2010; Newell-Fugate et al., 2014; Owen et al., 2013; Padilla et al., 2013; Payne et al., 2010; Pedersen et al., 2012; Rodgaard et al., 2013; Sabe et al., 2014b; Sham et al., 2014; Sturek et al., 2007; Talbott et al., 2006; Toedebusch et al., 2014; Trasino et al., 2013; Trask et al., 2012; Wastney et al., 2013; Witczak et al., 2005; Zhang et al., 2013)
2. Insulin resistance	No	Yes	(Bell et al., 2010; Dincer, 2011; Dyson et al., 2006; Edwards et al., 2010; Elmadhun et al., 2013; Faris et al., 2012; Fullenkamp et al., 2011; Habegger et al., 2012; Handa et al., 2014a; Handa et al., 2014b; Handa et al., 2014c; Kreutz et al., 2011; Lassaletta et al., 2012; Lee et al., 2009; Li et al., 2012; Li et al., 2011; McKenney et al., 2014; Neeb et al., 2010; Newell-Fugate et al., 2014; Otis et al., 2003; Padilla et al., 2013; Pedersen et al., 2012; Potu et al., 2013; Sham et al., 2014; Trask et al., 2012; Witczak and Sturek2004; Zhang et al., 2013)
3. Glucose intolerance (or impaired glucose tolerance, [IGT])	No	Yes	(Bell et al., 2010; Bender et al., 2009; Berwick et al., 2013; Boullion et al., 2003; Bratz et al., 2008; Dincer, 2011; Dixon et al., 2002; Dyson et al., 2006; Edwards et al., 2010; Elmadhun et al., 2014a; Faris et al., 2012; Fullenkamp et al., 2011; Handa et al., 2014a; Handa et al., 2014b; Handa et al., 2014c; Hanhineva et al., 2013; Kreutz et al., 2011; Lassaletta et al., 2012; Lee et al., 2009; Li et al., 2012; McKenney et al., 2014; Mokelke et al., 2003; Neeb et al., 2010; Newell-Fugate et al., 2014; Otis et al., 2003; Payne et al., 2010; Potu et al., 2013; Sabe et al., 2014b; Sham et al., 2014; Trask et al., 2012; Witczak et al., 2005; Witczak et al., 2006; Witczak and Sturek2004)
4. Dyslipidemia (↑LDL/HDL)	Yes	Yes	(Bell et al., 2010; Berwick et al., 2012; Berwick et al., 2013; Bratz et al., 2008; Clark et al., 2011; Dixon et al., 2002; Dyson et al., 2006; Edwards et al., 2010; Fullenkamp et al., 2011; Hanhineva et al., 2013; Kreutz et al., 2011; Lassaletta et al., 2012; Lee et al., 2003; Lee et al., 2009; Li et al., 2011; Long et al., 2010a; Long et al.,

			2010b; McKenney et al., 2014; Moberly et al., 2013; Neeb et al., 2010; Owen et al., 2013; Padilla et al., 2013; Potu et al., 2013; Rector et al., 2003; Trasino et al., 2013; Trask et al., 2012; Witczak et al., 2006; Zhang et al., 2013)
5. Dyslipidemia (↑ triglycerides)	No	Yes	(Bell et al., 2010; Bratz et al., 2008; Clark et al., 2011; Dincer, 2011; Dixon et al., 2002; Dyson et al., 2006; Edwards et al., 2010; Fullenkamp et al., 2011; Handa et al., 2014a; Hill et al., 2003; Kreutz et al., 2011; Lassaletta et al., 2012; Lee et al., 2009; Long et al., 2010a; McKenney et al., 2014; Moberly et al., 2013; Mokelke et al., 2003; Newell-Fugate et al., 2014; Payne et al., 2010; Potu et al., 2013; Rector et al., 2003; Trask et al., 2012; Witczak et al., 2005; Witczak and Sturek2004; Zhang et al., 2013)
6. Hypertension	No	Yes	(Berwick et al., 2012; Berwick et al., 2013; Bratz et al., 2008; Dincer, 2011; Dyson et al., 2006; Edwards et al., 2010; Elmadhun et al., 2014a; Faris et al., 2012; Handa et al., 2014c; Kreutz et al., 2011; Lassaletta et al., 2012; Lee et al., 2009; McKenney et al., 2014; Moberly et al., 2013; Otis et al., 2003; Payne et al., 2010; Trask et al., 2012; Zhang et al., 2013)
7. Cardiovascular disease, atherosclerosis	Yes	Yes	(Bender et al., 2009; Borbouse et al., 2009; Borbouse et al., 2010a; Borbouse et al., 2010b; Bratz et al., 2008; Chen et al., 2011; Dincer, 2011; Dixon et al., 2002; Dyson et al., 2006; Edwards et al., 2008; Edwards et al., 2010; Hainsworth et al., 2002; Korte et al., 2005; Langohr et al., 2008; Le et al., 2007; Lee et al., 2003; Lloyd et al., 2008; Long et al., 2010a; Mokelke et al., 2003; Mokelke et al., 2005; Neeb et al., 2010; Payne et al., 2010; Sturek, 2011; Turk et al., 2003; Wamhoff et al., 2002; Wang et al., 2008; Wang et al., 2009; Wang et al., 2013a; Ziegler et al., 2010) (Berwick et al., 2012; Berwick et al., 2013; Elmadhun et al., 2014a; Elmadhun et al., 2012; Elmadhun et al., 2014b; Hamamdzic and Wilensky2013; Handa et al., 2014b; Handa et al., 2014c; Huo et al., 2013; Kreutz et al., 2011; Lassaletta et al., 2012; Li et al., 2012; Li et al., 2011; Long et al., 2010b; McKenney et al., 2014; McKenney et al., 2015; Moberly et al., 2013; Owen et al., 2013; Paderi et al., 2011; Sabe et al., 2014a; Sabe et al., 2014b; Scott et al., 2013; Spence and Weaver2013; Trask et al., 2012; Wang et al., 2011a; Wang et al., 2011b; Wang et al., 2012; Wang et al., 2013b; Wastney et al., 2013; Zhang et al., 2013)

A very important message about Ossabaw miniature swine is the nearly ideal opportunity for achieving integration and translation to human clinical medicine. The need for a large animal, i.e. swine, model of the metabolic syndrome, instead of rodent models, was reinforced poignantly by European Union funded RETHINK project addressing the need for large animal research (Dolgin, 2010) and other position statements and initiatives to increase large animal research (Arner, 2005; Schwartz Longacre et al., 2011; Sipido et al., 2009). Despite the significant advances in mouse models that have been facilitated by the Animal Models for Diabetic Cardiovascular Complications (AMDCC) (Hsueh et al., 2007), it is our opinion and others (Seok et al., 2013) that the use of animal models in translational research requires large, more human-like animal models such as swine to be complete.

Genetic studies were performed on a repeating domain in the regulatory γ 3 subunit of the AMP-activated kinase (PRKAG3) gene. Hampshire pigs display a single amino acid difference at position 200 where arginine is mutated to glutamine (Arg200→ Gln). This gain-of-function genotype is associated with high muscle glycogen, low intramuscular fat, and overall leanness (Andersson, 2003; Milan et al., 2000). In contrast, sequencing of the PRKAG3 gene in Ossabaw Island pigs revealed the majority to be homozygous for a different mutation, Val199→ Ile, while the remainder of the pigs were heterozygous for the Val199→ Ile mutation and the wild-type allele Val199–Arg200 (Lloyd et al., 2006). The Val199→ Ile mutation is associated with impairment of AMP kinase enzyme activity, low muscle glycogen, and increased intramuscular fat, consistent with the obese Ossabaw pig phenotype (Andersson, 2003; Ciobanu et al., 2001). Selective breeding created a distinct line of Ossabaw pigs that is homozygous for the wild-type AMP kinase allele (Chawla et al., 2013). Consistent with the pivotal role of AMP kinase in energy balance, the homozygous wild-type AMP kinase line tolerates myocardial ischemia substantially better than the homozygous Val199→ Ile mutation Ossabaw with impaired AMP kinase activity (Chawla et al., 2013).

Table A.32–Table A.34 in the appendix make systematic comparison of serum chemistry data from trapped pigs on Ossabaw Island and data derived from Yucatan and Ossabaw pigs housed long term (1 year) in a biomedical research facility on standard pig chow. Pigs were anesthetized with isoflurane to obtain blood samples for the latter group compared to the caval blood sampling that employed physical restraint for the clinical chemistry from trapped Ossabaw. For both breeds in captivity housed in the biomedical facility the anion gap, potassium, total bilirubin, creatine kinase, and CO_2 are normal compared to the trapped wild pigs, thus probably indicating a less stressful environment overall and less stressful blood sampling procedure. Notable differences are the increased triglycerides and glucose in Ossabaws compared to Yucatans, which reinforce the more extreme cardiometabolic risk factor profile of the Ossabaws. Another intriguing difference is the increased creatinine in Ossabaws, which suggests some mild renal impairment even under these controlled conditions. The decreased urea nitrogen is consistent with less muscle mass in the Ossabaw (Ezekwe and Martin, 1975; Hausman et al., 1983; Kasser et al., 1981) and argues against the increased creatinine being driven by possibly increased muscle mass in the Ossabaws. It is completely unknown whether the increased ability of the Ossabaw kidney to concentrate urine (Zervanos et al., 1983) for adaptation to high salt consumption renders it more susceptible to subsequent damage. Overall, there was no difference in hematology between Ossabaw and Yucatan pigs. The only striking value in both breeds is the low hematocrit of 27. This is explained entirely by the isoflurane anesthesia, as Ossabaws sampled in the conscious state had a hematocrit of 41.8 ± 2.6 (SD; N = 5), similar to conscious Yucatans in other studies.

SUMMARY AND CONCLUSIONS

Ossabaw swine were rediscovered as a valuable animal resource after the removal, in 2002, of feral swine from Ossabaw Island, following the first removal nearly 40 years ago. Ossabaw swine removed from the island must undergo a stringent quarantine to ensure health and absence of parasites and major infectious diseases. The pigs have thrived in captivity. The "thrifty genotype" has been maintained in captivity for almost 13 years and the analogy to modern day humans suggests that the genotype will continue to be maintained. Clearly, Ossabaw swine express the major components of the metabolic syndrome ("prediabetes," "cardiometabolic risk"), including extreme obesity, insulin resistance, impaired glucose tolerance, dyslipidemia, and hypertension. Selective breeding has derived more general robust features of metabolic syndrome and distinct

lines of the AMP kinase genotypes. This chapter has provided an overview of the evidence for metabolic properties and methods of assessment and has contrasted the Ossabaw with the characteristics of more genetically lean Yucatan swine and domestic swine. Vascular studies provide detailed methods and characterization of vascular anatomy and functional properties. Unique vascular calcification and excessive stenosis after coronary stenting suggest predisposition to vascular disease and utility of the Ossabaw swine model. Exercise training of obese pigs is described. These findings echo the consensus that pigs in general and Ossabaw swine specifically are anatomically and metabolically similar to humans. The cardiovascular system is almost indistinguishable from that of humans and knowledge gained has much relevance to human medicine. Thus, the Ossabaw pig provides a unique animal resource to gain insight into multiple, complex factors involved in development of obesity, metabolic syndrome (pre-diabetes), and type 2 diabetes in humans and the resulting morbidity and mortality from cardiovascular disease. It is hoped that the future will see more widespread availability and use of Ossabaw swine in biomedical research.

> **Note:** The attached DVD contains descriptions of methods, images, and video clips of various aspects of the study of the metabolic syndrome in Ossabaw Island minipigs (Figure 18.1–Figure 18.28). Complete figure legends are included with the images. The outlined titles as follows provide a guide to the illustrations on the DVD.

Figure 18.1 — Ossabaw Island pig and environment.

Figure 18.2 — Standard Ossabaw swine housing facility for biomedical research.

Figure 18.3 — Growth and adipose composition of lean and obese male Ossabaw pigs housed in biomedical research facility.

Figure 18.4 — Noninvasive imaging of adipose distribution in Ossabaw swine.

Figure 18.5 — Measurement of glucose regulation and cardiovascular parameters in conscious pig.

Figure 18.6 — Catheterization supplies and angiography equipment.

Figure 18.7 — Hind limb arteries, ventrodorsal view. Includes video clips 18.1–18.6.

Figure 18.8 — Hind limb, superficial femoral artery access for catheterization, and formation of collateral femoral arteries in ventrodorsal view. Includes video clips 18.7 and 18.8.

Figure 18.9 — Renal arteries in ventrodorsal view. Includes video clips 18.9 and 18.10.

Figure 18.10 — Major abdominal arteries in ventrodorsal view. Includes video clips 18.11 and 18.12.

Figure 18.11 — Forelimb and thoracic arteries in ventrodorsal view. Includes video clips 18.13 and 18.14.

Figure 18.12 — Left carotid and cerebral arteries in ventrodorsal view. Includes video clips 18.15 and 18.16.

Figure 18.13 — Schematic of heart and major epicardial coronary arteries and interventional devices.

Figure 18.14 — Heart and right coronary artery in ventral views. Includes video clips 18.17–18.20.

Figure 18.15 — Heart and left coronary arteries in ventral views. Includes video clips 18.21–18.26.

Figure 18.16 — Ventricular angiography and echocardiography. Includes video clip 18.27.

Figure 18.17 — Two-dimensional and M-mode echocardiograms. Includes video clip 18.28.

ACKNOWLEDGMENTS

REFERENCES

Andersson, L. 2003. Identification and characterization of AMPKg3 mutations in the pig. *Biochem. Soc. Trans.* 31:232–235.

Arner, P. 2005. Resistin: yet another adipokine tells us that men are not mice. *Diabetologia* 48:2203-2205.

Bell, L.N., L.Lee, R.Saxena, K.G.Bemis, M.Wang, J.L.Theodorakis, R.Vuppalanchi, M.Alloosh, M.Sturek, and N.Chalasani. 2010. Serum proteomic analysis of diet-induced steatohepatitis and metabolic syndrome in the Ossabaw miniature swine. *Am.J.Physiol.Gastrointest.Liver Physiol.* 298:G746-G754.

Bellinger, D.A., E.P. Merricks, and T.C. Nichols. 2006. Swine models of type 2 diabetes mellitus: insulin resistance, glucose tolerance, and cardiovascular complications. *ILAR J.* 47:243–258.

Bender, S.B., J.D.Tune, L.Borbouse, X.Long, M.Sturek, and M.H.Laughlin. 2009. Altered mechanism of adenosine-induced coronary arteriolar dilation in early-stage metabolic syndrome. *Exp.Biol.Med.* 234:683-692.

Berwick, Z.C., G.M.Dick, S.P.Moberley, M.C.Kohr, M.Sturek, and J.D.Tune. 2012. Contribution of voltage-dependent K$^+$ channels to metabolic control of coronary blood flow. *J.Mol.Cell.Cardiol.* 52:912-919.

Berwick, Z., G.Dick, H.O'Leary, S.Bender, A.Goodwill, S.Moberly, M.Owen, S.Miller, A.Obukhov, and J.Tune. 2013. Contribution of electromechanical coupling between KV and CaV1.2 channels to coronary dysfunction in obesity. *Basic Res Cardiol* 108:370-

Bergman, R.N., D.T. Finegood, and M. Ader. 1985. Assessment of insulin sensitivity *in vivo*. *Endocr. Rev.* 6:45–86.

Bonin, E., A.Mariani, J.Swain, J.Bingener, K.Sumiyama, M.Knipschield, T.Sebo, and C.Gostout. 2012. Laparoscopic ultrasound-assisted liposuction for lymph node dissection: a pilot study. *Surg.Endosc.* (In press):1-8.

Borbouse, L., G.M.Dick, S.Asano, S.B.Bender, U.D.Dincer, G.A.Payne, Z.P.Neeb, I.N.Bratz, M.Sturek, and J.D.Tune. 2009. Impaired function of coronary BK$_{Ca}$ channels in metabolic syndrome. *Am.J.Physiol.Heart Circ.Physiol.* 297:H1629-H1637.

Borbouse, L., G.M.Dick, G.A.Payne, Z.C.Berwick, Z.P.Neeb, M.Alloosh, I.N.Bratz, M.Sturek, and J.D.Tune. 2010a. Metabolic syndrome reduces the contribution of K$^+$ channels to ischemic coronary vasodilation. *Am.J.Physiol.Heart Circ.Physiol.* 298:H1182-H1189.

Borbouse, L., G.M.Dick, G.A.Payne, B.D.Payne, M.C.Svendsen, Z.P.Neeb, M.Alloosh, I.N.Bratz, M.Sturek, and J.D.Tune. 2010b. Contribution of BK$_{Ca}$ channels to local metabolic coronary vasodilation: effects of metabolic syndrome. *Am.J.Physiol.Heart Circ.Physiol.* 298:H966-H973.

Borkan, G., S. Gerzof, A. Robbins, D. Hults, C. Silbert, and J. Silha. 1982. Assessment of abdominal fat content by computed tomography. *Am. J. Clin. Nutr.* 36:172–177.

Boullion, R.D., E.A. Mokelke, B.R. Wamhoff, C.R. Otis, J. Wenzel, J.L. Dixon, and M. Sturek. 2003. Porcine model of diabetic dyslipidemia: insulin and feed algorithms for mimicking diabetes in humans. *Comp. Med.* 53:42–52.

Bratz, I.N., G.M.Dick, J.D.Tune, J.M.Edwards, Z.P.Neeb, U.D.Dincer, and M.Sturek. 2008. Impaired capsaicin-induced relaxation of coronary arteries in a porcine model of the metabolic syndrome. *Am.J.Physiol.: Heart Circ.Physiol.* 294:H2489-H2496.

Brisbin, Jr.I.L. and J.J. Mayer. 2001. Problem pigs in a poke: a good pool of data. *Science* 294:1280–1281.

Buhlinger, C.A., P.J. Wangsness, R.J. Martin, and J.H. Ziegler. 1978. Body composition, *in vitro* lipid metabolism and skeletal muscle characteristics in fast-growing, lean and in slow-growing, obese pigs at equal age and weight. *Growth* 42:225–236.

Chen, H.Y., A.K.Sinha, J.S.Choy, H.Zheng, M.Sturek, B.Bigelow, D.L.Bhatt, and G.S.Kassab. 2011. Mis-sizing of stent promotes intimal hyperplasia: impact of endothelial shear and intramural stress. *Am J Physiol Heart Circ Physiol* 301:H2254-H2263.

Ciobanu, D., J. Bastiaansen, M. Malek, J. Helm, J. Woollard, G. Plastow, and M. Rothschild. 2001. Evidence for new aAlleles in the protein kinase adenosine monophosphate-aActivated g3-subunit gene associated with low glycogen content in pig skeletal muscle and improved meat quality. *Genetics* 159:1151–1162.

Clark, B.A., M.Alloosh, J.W.Wenzel, M.Sturek, and T.Y.Kostrominova. 2011. Effect of diet-induced obesity and metabolic syndrome on skeletal muscles of Ossabaw miniature swine. *Am.J.Physiol.Endocrinol.Metab.* 300:E848-E857.

Dincer, U.D. 2011. Cardiac â-adrenoceptor expression is markedly depressed in Ossabaw swine model of cardiometabolic risk. *International Journal of General Medicine* 4:493-499.

Dixon, J.L., J.D. Stoops, J.L. Parker, M.H. Laughlin, G.A. Weisman, and M. Sturek. 1999. Dyslipidemia and vascular dysfunction in diabetic pigs fed an atherogenic diet. *Arterioscler. Thromb. Vasc. Biol.* 19:2981–2992.

Dixon, J.L., S. Shen, J.P. Vuchetich, E. Wysocka, G. Sun, and M. Sturek. 2002. Increased atherosclerosis in diabetic dyslipidemic swine: protection by atorvastatin involves decreased VLDL triglycerides but minimal effects on the lipoprotein profile. *J. Lipid Res.* 43:1618–1629.

Dolgin, E. 2010. Minipig, minipig, let me in. *Nat Med* 16:1349-1349.

Dyson, M.C., M. Alloosh, R.D. Boullion, E.A. Mokelke, and M. Sturek. 2004. Glucose intolerance and insulin resistance in Ossabaw compared to Yucatan swine (abstract). *FASEB J.* 18:A1224.

Dyson, M., M. Alloosh, J.P. Vuchetich, E.A. Mokelke, and M. Sturek. 2006. Components of metabolic syndrome and coronary artery disease in female Ossabaw swine fed excess atherogenic diet. *Comp. Med.* 56:35–45.

Eckel, R.H., S.M. Grundy, and P.Z. Zimmet. 2005. The metabolic syndrome. *Lancet* 365:1415–1428.

Eckel, R.H., R. Kahn, R.M. Robertson, and R.A. Rizza. 2006. Preventing cardiovascular disease and diabetes: a call to action from the American Diabetes Association and the American Heart Association. *Circulation* 113:2943–2946.

Edwards, J.M., M.Alloosh, X.Long, G.M.Dick, P.G.Lloyd, E.A.Mokelke, and M.Sturek. 2008. Adenosine A_1 receptors in neointimal hyperplasia and in-stent stenosis in Ossabaw miniature swine. *Cor.Art.Dis.* 19:27-31.

Edwards, J.M., Z.P.Neeb, M.A.Alloosh, X.Long, I.N.Bratz, C.R.Peller, J.P.Byrd, S.Kumar, A.G.Obukhov, and M.Sturek. 2010. Exercise training decreases store-operated Ca^{2+} entry associated with metabolic syndrome and coronary atherosclerosis. *Cardiovasc.Res.* 85:631-640.

Edwards, J.M., J. Vuchetich, E.A. Mokelke, M. Alloosh, K.L. March, D. Hou, and M. Sturek. 2006. The Ossabaw swine model of the metabolic syndrome exhibits greater stenosis after coronary stenting than lean Yucatan swine (abstract). *FASEB J.* 20:A698.

Elmadhun, N.Y., A.A.Sabe, A.D.Lassaletta, L.M.Chu, K.Kondra, M.Sturek, and F.W.Sellke. 2014a. Metabolic syndrome impairs notch signaling and promotes apoptosis in chronically ischemic myocardium. *J.Thorac.Cardiovasc.Surg.* 148:1048-1055.

Elmadhun, N.Y., A.D.Lassaletta, L.M.Chu, Y.Liu, J.Feng, and F.W.Sellke. 2012. Atorvastatin increases oxidative stress and modulates angiogenesis in Ossabaw swine with the metabolic syndrome. *The Journal of Thoracic and Cardiovascular Surgery* 144:1486-1493.

Elmadhun, N.Y., A.D.Lassaletta, L.M.Chu, and F.W.Sellke. 2013. Metformin alters the insulin signaling pathway in ischemic cardiac tissue in a swine model of metabolic syndrome. *The Journal of Thoracic and Cardiovascular Surgery* 145:258-266.

Elmadhun, N.Y., A.A.Sabe, A.D.Lassaletta, L.M.Chu, and F.W.Sellke. 2014b. Metformin mitigates apoptosis in ischemic myocardium. *J Surg Res* 192:50-58.

Etherton, T.D. and P.M. Kris-Etherton. 1980. Characterization of plasma lipoproteins in swine with different propensities for obesity. *Lipids* 15:823–829.

Ezekwe, M.O. and R.J. Martin. 1975. Cellular characteristics of skeletal muscle in selected strains of pigs and mice and the unselected controls. *Growth* 39:95–106.

Ford, E.S., W.H. Giles, and A.H. Mokdad. 2004. Increasing prevalence of the metabolic syndrome among U.S. adults. *Diabetes Care* 27:2444–2449.

Faris, R.J., R.L.Boddicker, J.Walker-Daniels, J.Li, D.E.Jones, and M.E.Spurlock. 2012. Inflammation in Response to n3 Fatty Acids in a Porcine Obesity Model. *Comp.Med.* 62:495-503.

Flum, D.R., A.Devlin, A.S.Wright, E.Figueredo, E.Alyea, P.W.Hanley, M.K.Lucas, and D.E.Cummings. 2007. Development of a porcine Roux-en-Y gastric bypass survival model for the study of post-surgical physiology. *Obesity Surgery* 17:1332-1339.

Fullenkamp, A.M., L.N.Bell, R.D.Robbins, L.Lee, R.Saxena, M.Alloosh, J.E.Klaunig, R.G.Mirmira, M.Sturek, and N.Chalasani. 2011. Effect of different obesogenic diets on pancreatic histology in Ossabaw miniature swine. *Pancreas* 40:438-443.

Gal, D. and J.M.Isner. 1992. Atherosclerotic Yucatan microswine as a model for novel cardiovascular interventions and imaging. In Swine as Models in Biomedical Research. Swindle, M.M.; Moody, D.C.; Phillips, L.D. (Eds). Ames, IA: Iowas State University Press, pp. 118-140.

Grundy, S.M., H.B. Brewer, J.I. Cleeman, S.C. Smith, Jr., and C. Lenfant. 2004. Definition of the metabolic syndrome. *Circulation* 109:433–438.

Grundy, S.M., J.I. Cleeman, S.R. Daniels, K.A. Donato, R.H. Eckel, B.A. Franklin, D.J. Gordon, R.M. Krauss, P.J. Savage, S.C. Smith, Jr., J.A. Spertus, and F. Costa. 2005. Diagnosis and management of the metabolic syndrome: an American Heart Association/National Heart, Lung, and Blood Institute scientific statement. *Circulation* 112:2735–2752.

Habegger, K.M., B.A.Penque, W.Sealls, L.Tackett, L.N.Bell, E.K.Blue, P.J.Gallagher, M.Sturek, M.A.Alloosh, H.O.Steinberg, R.V.Considine, and J.S.Elmendorf. 2012. Fat-induced membrane cholesterol accrual provokes cortical filamentous actin destabilization and glucose transport dysfunction in skeletal muscle. *Diabetologia* 55:457-467.

Hainsworth, D.P., M.L. Katz, D.A. Sanders, D.N. Sanders, E.J. Wright, and M. Sturek. 2002. Retinal capillary basement membrane thickening in a porcine model of diabetes mellitus. *Comp. Med.* 52:523–529.

Hamamdzic, D. and R.L.Wilensky. 2013. Porcine models of accelerated coronary atherosclerosis: role of diabetes mellitus and hypercholesterolemia. *J.Diabetes Res.* 2013:761415.

Handa, R.K., A.P.Evan, B.A.Connors, C.D.Johnson, Z.Liu, M.Alloosh, M.Sturek, C.Evans-Molina, J.A.Mandeville, E.Gnessin, and J.E.Lingeman. 2014a. Shock wave lithotripsy targeting of the kidney and pancreas does not increase the severity of metabolic syndrome in a porcine model. *J.Urol.* 192:1257-1265.

Handa, R.K., C.D.Johnson, B.A.Connors, A.P.Evan, C.L.Phillips, and Z.Liu. 2014b. Shock wave lithotripsy does not impair renal function in a swine model of metabolic syndrome. *J.Endourol.* (In press)

Handa, R.K., Z.Liu, B.A.Connors, M.Alloosh, D.P.Basile, J.D.Tune, M.Sturek, A.P.Evan, and J.E.Lingeman. 2014c. Effect of renal shock wave lithotripsy on the development of metabolic syndrome in a juvenile swine model: a pilot study. *J.Urol.* 193:1-8.

Hanhineva, K., T.Barri, M.Kolehmainen, J.Pekkinen, J.Pihlajam+ñki, A.Vesterbacka, G.Solano-Aguilar, H.Mykk+ñnen, L.O.Dragsted, J.F.Urban, and K.Poutanen. 2013. Comparative non-targeted metabolite profiling of metabolic changes in tissues and bio-fluids in high-fat diet fed Ossabaw pig. *Journal of Proteome Research* 12:3980-3992.

Hausman, G.J., D.R. Campion, and G.B. Thomas. 1983. Semitendinosis muscle development in several strains of fetal and perinatal pigs. *J. Anim. Sci.* 57:1608–1617.

Hill, B.J.F., E.M.Price, J.L.Dixon, and M.Sturek. 2003. Increased calcium buffering in coronary smooth muscle cells from diabetic dyslipidemic pigs. *Atherosclerosis* 167:15-23.

Hsueh, W., E.D.Abel, J.L.Breslow, N.Maeda, R.C.Davis, E.A.Fisher, H.Dansky, D.A.McClain, R.McIndoe, M.K.Wassef, C.Rabadan-Diehl, and I.J.Goldberg. 2007. Recipes for Creating Animal Models of Diabetic Cardiovascular Disease. *Circ.Res.* 100:1415-1427.

Huo, Y., J.S.Choy, T.Wischgoll, T.Luo, S.D.Teague, D.L.Bhatt, and G.S.Kassab. 2013. Computed tomography-based diagnosis of diffuse compensatory enlargement of coronary arteries using scaling power laws. *J. R. Soc. Interface* 10:20121015.

Johnson, G.J., T.R.Griggs, and L.Badimon. 1999. The utility of animal models in the preclinical study of interventions to prevent human coronary artery restenosis: Analysis and recommendations. *Thromb.Haemost.* 81:835-843.

Kahn, R., J. Buse, E. Ferrannini, and M. Stern. 2005. The metabolic syndrome: time for a critical appraisal. Joint statement from the American Diabetes Association and the European Association for the Study of Diabetes. *Diabetologia* 48:1684–1699.

Kaser, S., E.A. Mokelke, M.N. Zafar, M.C. Dyson, and M. Sturek. 2004. Microvascular dysfunction after coronary stenting in a porcine model of the metabolic syndrome. *Diabetes* 53, Suppl. 2:A408–A409.

Kasser, T.R., R.J. Martin, J.H. Gahagan, and P.J. Wangsness. 1981. Fasting plasma hormones and metabolites in feral and domestic newborn pigs. *J. Anim. Sci.* 53:420–426.

Korte, F.S., E.A.Mokelke, M.Sturek, and K.S.McDonald. 2005. Exercise improves impaired ventricular function and alterations of cardiac myofibrillar proteins in diabetic dyslipidemic pigs. *J.Appl.Physiol.* 98:461-467.

Kreutz, R.P., M.Alloosh, K.Mansour, Z.P.Neeb, Y.Kreutz, D.A.Flockhart, and M.Sturek. 2011. Morbid obesity and metabolic syndrome in Ossabaw miniature swine are associated with increased platelet reactivity. *Diabetes Metab.Syndr.Obes.* 4:99-105.

Langohr, I.M., H.HogenEsch, G.W.Stevenson, and M.Sturek. 2008. Vascular-associated lymphoid tissue in swine (*sus scrofa*). *Comp.Med.* 58:168-173.

Larsen, M.O., C.B.Juhl, N.Porksen, C.F.Gotfredsen, R.D.Carr, U.Ribel, M.Wilken, and B.Rolin. 2005. Beta-cell function and islet morphology in normal, obese, and obese beta-cell mass-reduced Gottingen minipigs. *Am J Physiol Endocrinol Metab* 288:E412-E421.

Larsen, M.O., B.Rolin, K.Raun, L.Bjerre Knudsen, C.F.Gotfredsen, and T.Bock. 2007. Evaluation of beta-cell mass and function in the Gottingen minipig. *Diabetes, Obesity and Metabolism* 9, Suppl. 2:170-179.

Larsen, M.O., B.Rolin, M.Wilken, R.D.Carr, and O.Svendsen. 2002. High-fat high-energy feeding impairs fasting glucose and increases fasting insulin levels in the Gottingen minipig: results from a pilot study. *Ann N Y Acad Sci.* 967:414-423.

Larsen, M.O., B.Rolin, J.Sturis, M.Wilken, R.D.Carr, N.Porksen, and C.F.Gotfredsen. 2006. Measurements of insulin responses as predictive markers of pancreatic beta-cell mass in normal and beta-cell-

        reduced lean and obese Gottingen minipigs in vivo. *Am J Physiol Endocrinol Metab* 290:E670-
        E677.

Lassaletta, A.D., L.M.Chu, M.P.Robich, N.Y.Elmadhun, J.Feng, T.A.Burgess, R.J.Laham, M.Sturek, and
        F.W.Sellke. 2012. Overfed Ossabaw swine with early stage metabolic syndrome have normal
        coronary collateral development in response to chronic ischemia. *Basic Res.Cardiol.* 107:243-

Le, T., I.M.Langohr, M.J.Locker, M.Sturek, and J.-X.Cheng. 2007. Label-free molecular imaging of
        atherosclerotic lesions using multimodal nonlinear optical microscopy. *J.Biomed.Opt.* 12:054007-

Lee, D.L., B.R.Wamhoff, L.C.Katwa, H.K.Reddy, D.J.Voelker, J.L.Dixon, and M.Sturek. 2003. Increased
        endothelin-induced Ca^{2+} signaling, tyrosine phosphorylation, and coronary artery disease in
        diabetic dyslipidemic swine are prevented by atorvastatin. *J.Pharmacol.Exp.Ther.* 306:132-140.

Lee, L., M.Alloosh, R.Saxena, W.Van Alstine, B.A.Watkins, J.E.Klaunig, M.Sturek, and N.Chalasani. 2009.
        Nutritional model of steatohepatitis and metabolic syndrome in the Ossabaw miniature swine.
        Hepatology 50:56-67.

Li, Z.L., J.R.Woollard, B.Ebrahimi, J.A.Crane, K.L.Jordan, A.Lerman, S.M.Wang, and L.O.Lerman. 2012.
        Transition From Obesity to Metabolic Syndrome Is Associated With Altered Myocardial
        Autophagy and Apoptosis. *Arterioscler.Thromb.Vasc.Biol.* 32:1132-1141.

Li, Z., J.R.Woollard, S.Wang, M.J.Korsmo, B.Ebrahimi, J.P.Grande, S.C.Textor, A.Lerman, and
        L.O.Lerman. 2011. Increased glomerular filtration rate in early metabolic syndrome is associated
        with renal adiposity and microvascular proliferation. *American Journal of Physiology - Renal
        Physiology* 301:F1078-F1087.

Lloyd, P.G., M. Fang, I.L. Brisbin, Jr., L. Andersson, and M. Sturek. 2006. AMP kinase gene mutation is
        consistent with a thrifty phenotype (metabolic syndrome) in a population of feral swine (abstract).
        FASEB J. 20:A299.

Lloyd, P.G., A.F.Sheehy, J.M.Edwards, E.A.Mokelke, and M.Sturek. 2008. Leukemia inhibitory factor is
        upregulated in coronary arteries of Ossabaw miniature swine after stent placement. *Cor.Art.Dis.*
        19:217-226.

Long, X., I.N.Bratz, M.Alloosh, J.M.Edwards, and M.Sturek. 2010a. Short-term exercise training prevents
        micro- and macrovascular disease following coronary stenting. *J.Appl.Physiol.* 108:1766-1774.

Long, X., E.A.Mokelke, Z.P.Neeb, M.Alloosh, J.M.Edwards, and M.Sturek. 2010b. Adenosine receptor
        regulation of coronary blood flow in Ossabaw miniature swine. *J.Pharmacol.Exp.Ther.* 335:781-
        787.

Lowe, H.C., R.S.Schwartz, B.D.Mac Neill, I.K.Jang, M.Hayase, C.Rogers, and S.N.Oesterle. 2003. The
        porcine coronary model of in-stent restenosis: current status in the era of drug-eluting stents.
        Catheterization and Cardiovascular Interventions 60:515-523.

Martin, R.J. and J.H. Herbein. 1976. A comparison of the enzyme levels and the in vitro utilization substrates
        for lipogenesis in pair-fed lean and obese pigs. *Proc. Soc. Exp. Biol. Med.* 151:231–235.

Martin, R.J., J.L. Gobble, T.H. Hartsock, H.B. Graves, and J.H. Ziegler. 1973. Characterization of an obese
        syndrome in the pig. *Proc. Soc. Exp. Biol. Med.* 143:198–203.

Mayer, J.J. and I.L. Brisbin, Jr. 1991. *Wild Pigs of the United States: Their History, Morphology, and
        Current Status,* Athens, GA: University of Georgia Press.

Mattern, H.M., P.G.Lloyd, M.Sturek, and C.D.Hardin. 2007. Gender and genetic differences in bladder
        smooth muscle PPAR mRNA in a porcine model of the metabolic syndrome. *Mol.Cell.Biochem.*
        302:43-49.

McGill, H.C., Jr., A. McMahan, E.E. Herderick, A.W. Zieske, G.T. Malcom, R.E. Tracy, J.P. Strong, and
        Pathobiological Determinants of Atherosclerosis in Youth (PDAY) Research Group. 2002. Obesity
        accelerates the progression of coronary atherosclerosis in young men. *Circulation* 105:2712–2718.

McKenney, M.L., K.A.Schultz, J.H.Boyd, J.P.Byrd, M.Alloosh, S.D.Teague, A.A.Arce-Esquivel, J.N.Fain,
        M.H.Laughlin, H.S.Sacks, and M.Sturek. 2014. Epicardial adipose excision slows the progression
        of porcine coronary atherosclerosis. *J.Cardiothorac.Surg.* 9:2-

McKenney, M.L., P.R.Territo, A.Salavati, S.Houshmand, S.Persohn, Y.Liang, M.Alloosh, S.M.Moe,
        C.M.Weaver, A.Alavi, and M.Sturek. 2015. ^{18}F-NaF positron emission tomography imaging of
        early coronary artery calcification. *JACC Cardiovasc.Imaging* (In press)

Milan, D., J.T. Jeon, C. Looft, V. Amarger, A. Robic, M. Thelander, C. Rogel-Gaillard, S. Paul, N.
        Iannuccelli, L. Rask, H. Ronne, K. Lundström, N. Reinsch, J. Gellin, E. Kalm, P.L. Roy, P. Chardon,
        and L. Andersson. 2000. A mutation in PRKAG3 associated with excess glycogen content in pig
        skeletal muscle. *Science* 288:1248–1251.

Moberly, S., K.Mather, Z.Berwick, M.Owen, A.Goodwill, E.Casalini, G.Hutchins, M.Green, Y.Ng, R.Considine, K.Perry, R.Chisholm, and J.Tune. 2013. Impaired cardiometabolic responses to glucagon-like peptide 1 in obesity and type 2 diabetes mellitus. *Basic Res Cardiol* 108:365-

Mokdad, A., E. Ford, B. Bowman, D. Nelson, M. Engelgau, F. Vinicor, and J. Marks. 2001. The continuing increase of diabetes in the U.S. *Diabetes Care* 24:412–412.

Mokelke, E.A., Q. Hu, M. Song, L. Toro, H.K. Reddy, and M. Sturek. 2003. Altered functional coupling of coronary K^+ channels in diabetic dyslipidemic pigs is prevented by exercise. *J. Appl. Physiol.* 95:1179–1193.

Mokelke, E.A., N.J. Dietz, D.M. Eckman, M.T. Nelson, and M. Sturek. 2005a. Diabetic dyslipidemia and exercise affect coronary tone and differential regulation of conduit and microvessel K^+ current. *Am. J. Physiol. Heart Circ. Physiol.* 288:H1233–H1241.

Mokelke, E.A., R. Misra, and M. Sturek. 2005b. Caspase-3 levels are elevated in myocardium of hypercholesterolemic Ossabaw minipigs (abstract). *Diabetes* 54, Suppl. 1:A433.

Neel, J.V. 1962. Diabetes mellitus: a "thrifty" genotype rendered detrimental by "progress"' *Am. J. Hum. Genet.* 14:353–362.

Neeb, Z.P., J.M.Edwards, M.A.Alloosh, X.Long, E.A.Mokelke, and M.Sturek. 2010. Metabolic syndrome and coronary artery disease in Ossabaw compared with Yucatan swine. *Comp.Med.* 60:300-315.

Newell-Fugate, A.E., J.N.Taibl, S.G.Clark, M.Alloosh, M.Sturek, and R.L.Krisher. 2014. Effects of diet-induced obesity on metabolic parameters and reproductive function in female Ossabaw minipigs. *Comp.Med.* 64:44-49.

Otis, C.R., B.R.Wamhoff, and M.Sturek. 2003. Hyperglycemia-induced insulin resistance in diabetic dyslipidemic Yucatan swine. *Comp.Med.* 53:53-64.

Owen, M.K., F.A.Witzmann, M.L.McKenney, X.Lai, Z.C.Berwick, S.P.Moberly, M.Alloosh, M.Sturek, and J.D.Tune. 2013. Perivascular adipose tissue potentiates contraction of coronary vascular smooth muscle: influence of obesity. *Circulation* 128:9-18.

Paderi, J.E., K.Stuart, M.Sturek, K.Park, and A.Panitch. 2011. The inhibition of platelet adhesion and activation on collagen during balloon angioplasty by collagen-binding peptidoglycans. *Biomaterials* 32:2516-2523.

Padilla, J., N.T.Jenkins, S.Lee, H.Zhang, J.Cui, M.Y.Zuidema, C.Zhang, M.A.Hill, J.W.Perfield, J.A.Ibdah, F.W.Booth, J.W.Davis, M.H.Laughlin, and R.S.Rector. 2013. Vascular transcriptional alterations produced by juvenile obesity in Ossabaw swine. *Physiol.Genomics* 45:434-446.

Panepinto, L.M., R.W.Phillips, N.W.Westmoreland, and J.L.Cleek. 1982. Influence of genetics and diet on the development of diabetes in Yucatan miniature swine. *J.Nutr.* 112:2307-2313.

Payne, G.A., L.Borbouse, S.Kumar, Z.Neeb, M.Alloosh, M.Sturek, and J.D.Tune. 2010. Epicardial perivascular adipose-derived leptin exacerbates coronary endothelial dysfunction in metabolic syndrome via a protein kinase C-â pathway. *Arterioscler.Thromb.Vasc.Biol.* 30:1711-1717.

Pedersen, R., H.-C.Ingerslev, S.C.Salicio, M.Sturek, M.Alloosh, B.O.Christoffersen, S.G.Moesgaard, N.Larsen, and M.Boye. 2012. Characterization of gut microbiota in Ossabaw and Göttingen minipigs as models of obesity and metabolic syndrome. *PLoS One* 8:e56612-

Phillips, R.W., L.M.Panepinto, R.Spangler, and N.Westmoreland. 1982a. Yucatan miniature swine as a model for the study of human diabetes-mellitus. *Diabetes* 31:30-36.

Phillips, R.W., N.Westmoreland, L.Panepinto, and G.L.Case. 1982b. Dietary effects on metabolism of Yucatan miniature swine selected for low and high glucose utilization. *J.Nutr.* 112:104-111.

Potu, R., H.Lu, O.Adeola, and K.Ajuwon. 2013. Metabolic markers in Ossabaw pigs fed high fat diets enriched in regular or low alpha-linolenic acid soy oil. *Nutrition & Metabolism* 10:27-

Rector, R.S., T.R.Thomas, Y.Liu, K.K.Henderson, D.A.Holiman, G.Y.Sun, and M.Sturek. 2003. Effect of exercise on postprandial lipemia following a higher calorie meal in Yucatan miniature swine. *Metabolism* 53:1021-1026.

Rodgaard, T., J.Stagsted, B.O.Christoffersen, S.Cirera, S.G.Moesgaard, M.Sturek, M.Alloosh, and P.M.H.Heegaard. 2013. Orosomucoid expression profiles in liver, adipose tissues and serum of lean and obese domestic pigs, Göttingen minipigs and Ossabaw minipigs. *Vet.Immunol.Immunopathol.* 151:325-330.

Sabe, A.A., N.Y.Elmadhun, A.A.Sadek, R.S.Dalal, L.M.Chu, C.Bianchi, and F.W.Sellke. 2014a. Atorvastatin regulates apoptosis in chronically ischemic myocardium. *J.Card.Surg.* 30:218-223.

Sabe, A.A., N.Y.Elmadhun, A.A.Sadek, L.M.Chu, C.Bianchi, and F.W.Sellke. 2014b. Differential effects of atorvastatin on autophagy in ischemic and nonischemic myocardium in Ossabaw swine with metabolic syndrome. *The Journal of Thoracic and Cardiovascular Surgery* 148:3172-3178.

Schwartz Longacre, L., R.A.Kloner, A.E.Arai, C.P.Baines, R.Bolli, E.Braunwald, J.Downey, R.J.Gibbons, R.A.Gottlieb, G.Heusch, R.B.Jennings, D.J.Lefer, R.M.Mentzer, E.Murphy, M.Ovize, P.Ping, K.Przyklenk, M.N.Sack, R.S.Vander Heide, J.Vinten-Johansen, and D.M.Yellon. 2011. New Horizons in Cardioprotection. *Circulation* 124:1172-1179.

Schwartz, R.S. and E.R.Edelman. 2002. Drug-eluting stents in preclinical studies. Recommended evaluation from a consensus group. *Circulation* 106:1867-1873.

Scott, R.A., J.E.Paderi, M.Sturek, and A.Panitch. 2013. Decorin mimic inhibits vascular smooth muscle proliferation and migration. *PLoS One* 8:e82456-

Seok, J., H.S.Warren, A.G.Cuenca, M.N.Mindrinos, H.V.Baker, W.Xu, D.R.Richards, G.P.McDonald-Smith, H.Gao, L.Hennessy, C.C.Finnerty, C.M.L+¦pez, S.Honari, E.E.Moore, J.P.Minei, J.Cuschieri, P.E.Bankey, J.L.Johnson, J.Sperry, A.B.Nathens, T.R.Billiar, M.A.West, M.G.Jeschke, M.B.Klein, R.L.Gamelli, N.S.Gibran, B.H.Brownstein, C.Miller-Graziano, S.E.Calvano, P.H.Mason, J.P.Cobb, L.G.Rahme, S.F.Lowry, R.V.Maier, L.L.Moldawer, D.N.Herndon, R.W.Davis, W.Xiao, R.G.Tompkins, and L.S.C.R.P.the Inflammation and Host Response to Injury. 2013. Genomic responses in mouse models poorly mimic human inflammatory diseases. *Proceedings of the National Academy of Sciences* 110:3507-3512.

Sham, J.G., V.V.Simianu, A.S.Wright, S.D.Stewart, M.Alloosh, M.Sturek, D.E.Cummings, and D.R.Flum. 2014. Evaluating the mechanisms of improved glucose homeostasis after bariatric surgery in Ossabaw miniature swine. *J.Diabetes Res.* 2014:526972-

Sheehy, A., E.A. Mokelke, P.G. Lloyd, J. Sturek, and M. Sturek. 2006. Reduced expression of leukemia inhibitory factor correlates with coronary atherosclerosis in the metabolic syndrome (abstract). *FASEB J.* 20:A698.

Sipido, K.R., A.Tedgui, S.D.Kristensen, G.Pasterkamp, H.Schunkert, M.Wehling, P.G.Steg, W.Eisert, F.Rademakers, B.Casadei, V.Fuster, E.Cerbai, G.Hasenfuss, F.Fernandez-Aviles, D.Garcia-Dorado, M.Vidal, M.Hallen, and V.Dambrauskaite. 2009. Identifying needs and opportunities for advancing translational research in cardiovascular disease. *Cardiov.Res.* 83:425-435.

Spence, L.A. and C.M.Weaver. 2013. Calcium intake, vascular calcification, and vascular disease. *Nutr.Rev.* 71:15-22.

Stribling, H.L., Jr., I.L. Brisbin, J.R. Sweeney, and L.A. Stribling. 1984. Body fat reserves and their prediction in two populations of feral swine. *J. Wildl. Manage.* 48:635–639.

Sturek, M. 2011. Ca^{2+} regulatory mechanisms of exercise protection against coronary artery disease in metabolic syndrome and diabetes. *J.Appl.Physiol.* 111:573-586.

Talbott, C., T.See, P.Kaminsky, D.Bixby, M.Sturek, I.L.Brisbin, Jr., and C.Kadzere. 2006. Enhancing pork flavor and fat quality with swine raised in sylvan systems: potential niche-market application for the Ossabaw hog. *Renewable Ag.Food Systems* 21:183-191.

Toedebusch, R.G., M.D.Roberts, K.D.Wells, J.Company, K.M.Kanosky, J.Padilla, N.T.Jenkins, J.W.Perfield, J.A.Ibdah, F.W.Booth, and R.S.Rector. 2014. Unique transcriptomic signature of omental adipose tissue in Ossabaw swine: a model of childhood obesity. *Physiol.Genomics* 46:362-375.

Touchard, A.G. and R.S.Schwartz. 2006. Preclinical restenosis models: challenges and successes. *Toxicol.Pathol.* 34:11-18.

Trasino, S.E., H.D.Dawson, J.Urban, T.T.Y.Wang, and G.Solano-Aguilar. 2013. Feeding probiotic Lactobacillus paracasei to Ossabaw pigs on a high-fat diet prevents cholesteryl-ester accumulation and LPS modulation of the Liver X receptor and inflammatory axis in alveolar macrophages. *The Journal of Nutritional Biochemistry* 24:1931-1939.

Trask, A.J., P.S.Katz, A.P.Kelly, M.L.Galantowicz, M.J.Cismowski, T.A.West, Z.P.Neeb, Z.C.Berwick, A.G.Goodwill, M.Alloosh, J.D.Tune, M.Sturek, and P.A.Lucchesi. 2012. Dynamic micro- and macro-vascular remodeling in coronary circulation of obese Ossabaw pigs with metabolic syndrome. *J.Appl.Physiol.* 113:1128-1140.

Turk, J.R., J.A.Carroll, M.H.Laughlin, T.R.Thomas, J.Casati, D.K.Bowles, and M.Sturek. 2003. C-reactive protein correlates with macrophage accumulation in coronary arteries of hypercholesterolemic pigs. *J.Appl.Physiol.* 95:1301-1304.

Wamhoff, B.R., J.L.Dixon, and M.Sturek. 2002. Atorvastatin treatment prevents alterations in coronary smooth muscle nuclear Ca^{2+} signaling associated with diabetic dyslipidemia. *J.Vasc.Res.* 39:208-220.

Wang, H.-W., N.Chai, P.Wang, S.Hu, W.Dou, D.Umulis, L.V.Wang, M.Sturek, R.Lucht, and J.-X.Cheng. 2011a. Label-free bond-selective imaging by listening to vibrationally excited molecules. *Phys.Rev.Lett.* 106:238106-

Wang, H.-W., I.M.Langohr, M.Sturek, and J.-X.Cheng. 2009. Imaging and quantitative analysis of atherosclerotic lesions by CARS-based multimodal nonlinear optical microscopy. *Arterioscler.Thromb.Vasc.Biol.* 29:1342-1348.

Wang, H.-W., V.Simianu, M.J.Locker, J.-X.Cheng, and M.Sturek. 2011b. Stent-induced coronary artery stenosis characterized by multimodal nonlinear optical microscopy. *J.Biomed.Opt.* 16:021110-

Wang, H.-W., V.Simianu, M.J.Locker, M.Sturek, and J.-X.Cheng. 2008. Imaging arterial cells, atherosclerosis, and restenosis by multimodal nonlinear optical microscopy. *Proc.SPIE* 6860:68600W-

Wang, H.-W., M.Sturek, and J.-X.Cheng. 2013a. Applications of coherent anti-Stokes Raman spectroscopy imaging to cardiovascular diseases:537-546.

Wang, P., J.Li, P.Wang, C.-R.Hu, D.Zhang, M.Sturek, and J.-X.Cheng. 2013b. Label-free quantitative imaging of cholesterol in intact tissues by hyperspectral stimulated Raman scattering microscopy. *Angew.Chem.Int.Ed.Engl.* 52:13042-13046.

Wang, P., H.-W.Wang, M.Sturek, and J.-X.Cheng. 2012. Bond-selective imaging of deep tissue through the optical window between 1600 and 1850 nm. *J.Biophotonics* 5:25-32.

Wangsness, P.J., R.J. Martin, and J.H. Gahagan. 1977. Insulin and growth hormone in lean and obese pigs. *Am. J. Physiol.* 233:E104–E108.

Wastney, M., W.H.Lee, G.S.Jackson, M.Alloosh, M.Sturek, P.Lachick, M.Peacock, B.Martin, and C.M.Weaver. 2013. Soft tissue calcification in the Ossabaw miniature pig: experimental and kinetic modeling studies. *Osteoporos.Int.* 24:2123-2126.

Weiss, G.M., D.G. Topel, D.G. Siers, and R.C. Ewan. 1974. Influence of adrenergic blockage upon some endocrine and metabolic parameters in a stress-susceptible and a fat strain of swine. *J. Anim. Sci.* 38:591–597.

Witczak, C.A. and M. Sturek. 2004. Exercise prevents diabetes-induced impairment in superficial buffer barrier in porcine coronary smooth muscle. *J. Appl. Physiol.* 96:1069–1079.

Witczak, C.A., E.A. Mokelke, R.D. Boullion, J. Wenzel, D.H. Keisler, and M. Sturek. 2005. Noninvasive measures of body fat percentage in male Yucatan swine. *Comp. Med.* 55:445–451.

Witczak, C.A., B.R.Wamhoff, and M.Sturek. 2006. Exercise training prevents Ca^{2+} dysregulation in coronary smooth muscle from diabetic dyslipidemic Yucatan swine. *J.Appl.Physiol.* 101:752-762.

Zafar, M.N., E.A. Mokelke, S. Kaser, and M. Sturek. 2004. C-reactive protein is predictive of in-stent neointimal hyperplasia, but not atheroma at baseline, in swine with the metabolic syndrome (abstract). *Arterioscler. Thromb. Vasc. Biol.* 24:103.

Zervanos, S.M., W.D. McCort, and H.B. Graves. 1983. Salt and water balance of feral versus domestic Hampshire hogs. *Physiol. Zool.* 56:67–77.

Zhang, X., Z.L.Li, J.R.Woollard, A.Eirin, B.Ebrahimi, J.A.Crane, X.Zhu, A.Pawar, J.D.Krier, K.L.Jordan, H.Tang, S.C.Textor, A.Lerman, and L.O.Lerman. 2013. Obesity-metabolic derangement preserves hemodynamics but promotes intra-renal adiposity and macrophage infiltration in swine renovascular disease. *American Journal of Physiology - Renal Physiology* 305:F265-F276.

Ziegler, M.A., M.R.DiStasi, R.G.Bills, S.J.Miller, M.Alloosh, M.P.Murphy, A.G.Akingba, M.Sturek, M.C.Dalsing, and J.L.Unthank. 2010. Marvels, mysteries, and misconceptions of vascular compensation to peripheral artery occlusion. *Microcirculation* 17:1-18.

Zygmont, S.M., V.F. Nettles, E.B. Shotts, W.A. Carmen, and B.O. Blackburn. 1982. Brucellosis in wild swine: a serologic and bacteriologic survey in the southeastern United States and Hawaii. *J. Am. Vet. Med. Assoc.* 181:1285-1287.

APPENDIX

Table A.9. Feed composition and amount for normal growth of Ossabaw miniature swine

Age (months)	Feed Type	Feed (g)	kcal
Up to 1-1.5	Typical Creep Feed or LabDiet Mini-Pig Starter #5080	Ad Libitum	up to ~920
1.5	LabDiet Mini-Pig Grower #5L80 or Starter #5080	270	920
2	Lab Diet Mini-Pig Grower #5L80	300	990
3	Lab Diet Mini-Pig Grower #5L80	350	1155
4	Lab Diet Mini-Pig Grower #5L80	400	1320
5	Lab Diet Mini-Pig Grower #5L80	450	1485
6	Lab Diet Mini-Pig Grower #5L80	500	1650
7	Lab Diet Mini-Pig Grower #5L80	550	1815
8	LabDiet Mini-pig Breeder #5082 or Mini-Pig Grower #5L80	800	2400
>8	LabDiet Mini-pig Breeder #5082 or Mini-Pig Grower #5L80	~800	~2400-2700

Table A.28. Hematology for male, adult Yucatan and Ossabaw miniature swine

		Yucatan				Ossabaw			
		Mean	SD	Min	Max	Mean	SD	Min	Max
Erythrocytes	(x10^{6}/mL)	4.4	0.2	4.0	4.7	4.8	0.5	4.2	5.4
Hematocrit[1]	%	26.6	1.6	24.0	29.0	26.6	2.7	23.0	29.0
Hemoglobin	g/dL	9.2	0.7	8.1	10.3	9.2	1.1	7.8	10.2
Mean corpuscular volume, MCV	fL	60.7	2.2	58.0	64.0	55.7	1.3	54.0	57.0
Mean Corpuscular Hemoglobin, MCH	pg	21.1	1.1	19.9	22.6	19.1	0.6	18.6	20.0
Mean Corpuscular Hemoglobin Concentration, MCHC	g/dL	34.6	0.6	33.9	35.5	34.5	0.7	33.6	35.2
Leukocytes	(x10^{3}/mL)	8.2	1.4	6.5	10.7	10.5	2.2	8.0	13.8
Semented Neutrophils	(x10^{3}/mL)	3.43	0.88	2.48	4.92	4.32	1.58	2.68	6.90
Banded Neutrophils[2]	(x10^{3}/mL)	0.09	0.02	0.08	0.11	0	0	0	0
Lymphocytes	(x10^{3}/mL)	4.54	0.91	3.49	6.08	5.29	1.07	3.29	6.21
Monocytes	(x10^{3}/mL)	0.29	0.17	0	0.50	0.79	0.44	0.37	1.40
Eosinophils	(x10^{3}/mL)	0.04	0.05	0	0.11	0.07	0.10	0	0.27
Basophils	(x10^{3}/mL)	0	0	0	0	0.11	0.20	0	0.40
Platelets[3]	(x10^{3}/mL)	427.1	83.8	300	553	562.0	150.3	422.0	692.0

N=7 per breed group, except were noted; age = ~12-15 mo. [1]Hematocrit under anesthesia.
[2]Undetectable in all Ossabaws; detectable in 3 Yucatans. [3]N=4 Ossabaw.

Table A.29. Clinical chemistry for male, adult trapped Ossabaw Island miniature swine					
Electrolytes		**Mean**	**SD**	**Min**	**Max**
Anion Gap	mmol/L	28.5	5.5	21	40
Calcium	mg/dL	9.6	1.3	7.5	11.5
Chloride	mmol/L	95.2	9.1	80.0	107.0
Magnesium	mg/dL	2.8	0.6	2.1	4.5
Phosphorus	mg/dL	7.2	1.3	4.8	9.5
Potassium	mmol/L	7.3	1.2	4.8	9.6
Sodium	mmol/L	139.1	13.5	117	157
Carbohydrate Metabolism					
Glucose	mg/dL	136.5	75.4	82	436
Liver Function a) Hepatocellular					
Alkaline Phosphatase, ALP	U/L	57.2	21.0	32.0	107.0
Aspartate Aminotranferase, AST	U/L	51.2	20.0	25	92
Gamma-Glutamyl Transferase, GGT	U/L	59.0	9.6	42	77
Liver Function b) Hepatobiliary					
Unconjugated Bilirubin	mg/dL	0.005	0.02	0	0.1
Total Bilirubin	mg/dL	0.27	0.16	0.1	0.6
Kidney Function					
Creatinine	mg/dL	1.8	0.4	1.1	2.7
Urea Nitrogen	mg/dL	8.2	2.4	4.0	13.0
Others					
Albumin	g/dL	3.6	0.6	2.7	4.6
Globulin	g/dL	3.8	0.4	3.1	4.6
Albumin/Globulin Ratio		0.94	0.16	0.59	1.19
Total Protein	g/dL	7.4	0.8	6.0	9.0
Creatine kinase	U/L	1031	638	179	2112
Total Cholesterol	mg/dL	77.9	23.7	45	127
Triglycerides	mg/dL	33.2	13.2	18	74
Total CO_2	mmol/L	22.8	3.1	17	30
Body Weight	kg	46.7	11.9	29.1	73.6

N=19; estimated age >9 mo.

Mean, standard deviation (SD), and minimum (Min) and maximum (Max) values and units of measure are provided.

Table A.30. Clinical chemistry for male, adult Yucatan and Ossabaw miniature swine									
		Yucatan				Ossabaw			
Electrolytes		**Mean**	**SD**	**Min**	**Max**	**Mean**	**SD**	**Min**	**Max**
Anion Gap	mmol/L	10.9	2.1	6.6	13.0	9.7	2.4	6.0	12.0
Calcium	mg/dL	10.0	0.44	9.5	10.6	10.0	0.18	9.8	10.2
Chloride	mmol/L	101.1	2.12	99.0	105.0	100.4	1.4	98.0	102.0
Magnesium	mg/dL	2.4	0.2	2.2	2.6	2.2	0.1	2.1	2.3
Phosphorus	mg/dL	6.63	0.5	6.4	7.2	7.1	0.4	6.5	7.5
Potassium	mmol/L	3.8	0.32	3.4	4.4	4.2	0.2	4.0	4.4
Sodium	mmol/L	142.7	2.1	139.0	145.0	142.0	1.5	140.0	143.0
Carbohydrate Metabolism									
Glucose	mg/dL	93.1	31.9	47	150	126.0	12.3	107	145
Liver Function a) Hepatocellular									
Alkaline Phosphatase, ALP	U/L	58.1	13.5	42.0	83.0	67.0	7.6	62.0	75.0
Aspartate Aminotranferase, AST	U/L	29.1	5.1	19	34	24.0	4.2	19.0	26.0
Gamma-Glutamyl Transferase, GGT	U/L	45.9	13.9	23	61	60.4	15.8	45.0	83.0
Liver Function b) Hepatobiliary									
Unconjugated Bilirubin	mg/dL	0.04	0.08	0.0	0.2	0	0	0	0
Total Bilirubin	mg/dL	0.11	0.04	0.1	0.3	0.1	0.0	0.1	0.1
Kidney Function									
Creatinine	mg/dL	1.3	0.1	1.1	1.5	1.7	0.3	1.1	1.9
Urea Nitrogen	mg/dL	15.1	2.4	11.0	18.0	10.7	2.6	7.0	14.0
Others									
Albumin	g/dL	3.3	0.2	2.9	3.5	3.4	0.3	3.1	3.7
Globulin	g/dL	3.0	0.2	2.9	3.2	2.8	0.2	2.6	3.0
Albumin/Globulin Ratio		1.11	0.15	0.94	1.4	1.20	0.08	1.13	1.35
Total Protein	g/dL	6.3	0.3	6.0	6.6	6.2	0.4	5.8	6.7
Creatine kinase	U/L	303.1	114.4	203.0	469.0	450.3	94.6	397.0	570.0
Total Cholesterol	mg/dL	73.3	12.0	45.0	108.0	90.6	16.2	56.0	142.0
Triglycerides	mg/dL	27.0	8.4	9.0	52.0	37.3	11.5	11.0	70.0
Total CO_2	mmol/L	33.3	1.11	32.0	35.0	35.4	3.2	32	40
Body Weight	kg	60.7	6.2	53.2	68.9	74.1	4.8	68.6	81.4
N=7 per breed group; age = ~12-15 mo.									

Mean, standard deviation (SD), and minimum (Min) and maxiumum (Max) values and units of measure are provided.

Table A.36. Visceral composition of male Yucatan and Ossabaw miniature swine

Breed	Control chow	46% kcal fat	75% kcal fat
	Diet		
Ossabaw (N =)	7	8	3
% Protein	12.2 ± 0.4	11.7 ± 0.3	9.9 ± 0.5
% Fat	19.9 ± 1.9	23.4 ± 0.8	28.9 ± 0.6
Yucatan (N =)	6	5	3
% Protein	13.2 ± 0.5	13.4 ± 0.5	11.9 ± 0.2
% Fat	12.5 ± 2.1	16.2 ± 2.8	20.3 ± 2.0

Values are mean ± standard error.

FIGURE CAPTIONS

Figure 18.1. Ossabaw Island pig and environment. A. Foraging for food in a coastal salt marsh. Inset: aerial image of Ossabaw Island (courtesy of Sandy West, Ossabaw Island, GA). B. Live oaks. C. Inland fresh water marsh. D. Inland salt water marsh. E. Trap for capturing feral Ossabaw swine. Inset: trapped pigs. F. Captive pigs. See also color images on CD.

Figure 18.2. Standard Ossabaw swine housing facility for biomedical research. See also color image on CD.

Figure 18.3. Growth and adipose composition of lean and obese male Ossabaw pigs housed in biomedical research facility. A. Body weight of Lean pigs fed a normal chow diet and Obese pigs fed excess atherogenic diet (Obesity Diet) starting at the time indicated by the arrow. B. Regression analysis of direct chemical measurement of visceral fat percentage vs. body weight of male Yucatan (N=12, circles) and Ossabaw (N=17, squares) pigs. Equations for prediction of % visceral fat (y) from body weight (x) and correlations (R) are given.

Figure 18.4. Non-invasive imaging of adipose distribution in Ossabaw swine. A. Computed tomography scan of female on standard pig chow maintenance diet. B. Computed tomography scan shows that obesity diet for 9 weeks elicits increase in adipose tissue (dark areas) in subcutaneous, retroperitoneal, and visceral regions. (Panels A and B are from Dyson et al. {11173} with permission.) Structures labeled apply to panel C-E, also. C. Computed tomography scan of female on obesity diet for 22 weeks shows further increase in adipose in all compartments. D. Magnetic resonance image of fat (bright components) in male on obesity diet for 22 weeks. E. Magnetic resonance image of water (bright components) in same male as panel D. Arrows in C, D, and E show visceral fat compartment.

Figure 18.5. Measurement of glucose regulation and cardiovascular parameters in conscious pig. A. in Panepinto low-stress restraint sling. (Modified from Otis et al. {11067} with permission.). Infusions are done in ear veins, while infusions and blood draws are done through percutaneous jugular catheters or vascular access ports. Blood pressure is monitored non-invasively with tail or forelimb cuff. Cardiac and vascular transcutaneous ultrasound, needle biopsies, fluorescein angiography of retinal vessels, rectal ultrasound, and other tests can be performed. B. Jugular catheter supplies. A-introducer / dilator, B-percutaneous needle (18 ga.) in protective sleeve, C-syringe, D-catheter, E1-proximal end of J-guidewire (0.038 inch [0.97 mm]), E2-distal end of J-guidewire, F-guidewire holder. C. Typical intravenous glucose tolerance test protocol showing blood glucose responses of lean and obese Ossabaw pigs. D. Plasma insulin responses from lean and obese pigs in panel C.

Figure 18.6. Catheterization supplies and angiography equipment. A. A-percutaneous transluminal coronary angioplasty guidewire (0.014 inch [0.36 mm] diameter), B-introducer for angioplasty guidewire insertion into hemostatic valve, C-torquer for grasping and turning angioplasty guidewire, D-saline supply line, E-blood pressure transducer line, F-contrast media supply line, G-syringe for injecting contrast media, H-hemostatic valve, I-3-way valve with extension tubing to hemostatic valve, J-3-way manifold, K-guiding catheter (Amplatz left, sizes 0.5-2.0; 7-8 F [2.33-2.67 mm], side holes), L-guidewire (0.038 inch [0.97 mm]) for guiding catheter, M-introducer (left side) and sheath with side port and 3-way valve, N-J guidewire (0.038 inch [0.97 mm]). B. C-arm configuration for right ventral oblique 30 degrees angulation. Vertical line denotes pure ventrodorsal orientation (0º from vertical). Thick shaded column angled 30 degrees right of pig from vertical shows area of x-ray detection. a-catheterization supplies in panel A on patient table. C. C-arm configuration for left ventral oblique 30 degrees angulation.

Same conditions as panel B, except that the thick shaded column shows area x-ray detection angled 30 degrees left of pig from vertical.

Figure 18.7. Hindlimb arteries, ventrodorsal view. Body weight of pig is 40 kg. A. Right distal superficial femoral and saphenous arteries. a-distal femur, b-stifle (knee) joint, c-lateral condyle of femur, d-medial condyle of femur, e-tibia, f-fibula, g-superficial femoral, h-saphenous, i-popliteal. Fine black lines and dark area peripheral to the lines indicate aperture that is adjusted to decrease x-ray in non-tissue areas. Spatial calibration is same for all panels. Image is brightness and contrast adjusted. **Video 18.1.** Perfusion of right distal femoral, saphenous, and popliteal. Note that all videos loop until stopped. B. Right superficial femoral and deep (profunda) femoral. a-hip joint, head of femur, b-femur, c-medial and lateral condyles of femur, d-gluteal artery, e-superficial femoral, f-deep (profunda) femoral, g-distal internal iliac branches, arrow-typical site for catheterization. **Video 18.2.** Perfusion of all arteries in panel B and numerous distal branches. C. Aorto-iliac bifurcation. a-os coxae bone, b-sacrum (part of vertebral column), c-aorta, d-external iliac, e-internal iliac, f-circumflex iliac, g-caudal (sacral) artery and branches, h-gluteal, i-deep (profunda) femoral, j-distal internal iliac, k-femoral. Spasm in segment of internal iliac is shown to the right of double arrows. **Video 18.3.** Perfusion of all arteries in panel C and numerous distal branches; pulsatile flow is especially noted in aorta. D. Aorto-iliac bifurcation of different pig than in panel C. Letters denote same structures as in panel C. Spasm in segment of internal iliac is shown to the left of double arrows. **Video 18.4.** Perfusion of all arteries in panel D and numerous distal branches; air bubble is visible distal to spasm in right internal iliac. E. Left distal superficial femoral and saphenous. Letters and lines denote same structures as in panel A. Image is brightness and contrast adjusted. **Video 18.5.** Perfusion of left distal femoral, saphenous, and popliteal. F. Left superficial femoral and deep (profunda) femoral. Letters denote same structures as in panel B. **Video 18.6.** Perfusion of all arteries in panel F and numerous distal branches; deep femoral angles acutely at its termination toward the superficial femoral.

Figure 18.8. Hindlimb, superficial femoral artery access for catheterization, and formation of collateral femoral arteries in ventrodorsal view. A. Right superficial femoral with guiding catheter inserted. Contrast media is injected only to the end of the guiding catheter. Spatial calibration is same for all panels. Body weight of pig is 40 kg. a-os coxae bone, b-sacrum (part of vertebral column), c-head of femur, hip joint, d-femur, e-tip to guidewire cranial to deep (profunda) femoral (not shown) branching medially off external iliac (not shown), f-tip to guiding catheter in superficial femoral, g-catheter insertion site. B. Injection of contrast media through guiding catheter in right superficial femoral. a-g are same as panel A, h-deep (profunda) femoral, i-left gluteal, right gluteal is absent because of guiding catheter occlusion, j-internal iliac, k-circumflex iliac, l-external iliac, m-superficial femoral. **Video 18.7.** Contrast media infusion through guiding catheter retrograde into superficial femoral with pronounced perfusion of right deep femoral (located medial to the catheter). C. Right deep (profunda) femoral artery collaterals 4 weeks after ligation of the superficial femoral. Image captured at the middle of contrast media injection into the aorto-iliac bifurcation, during which time the contrast fills mostly conduit arteries. Body weight of pig is 110 kg. a- head of femur, hip joint, b-femur, c-gluteal artery, d-deep (profunda) femoral artery, e-superficial femoral ligation site at arrow, f-former location of superficial femoral artery, g-"corkscrew" collateral directly below the letter g, double arrow-area of poor perfusion of contrast media in microvasculature. D. Same conditions as panel C, except the image captured at the end of contrast media injection in the aorto-iliac bifurcation, during which time the contrast fills mostly distal microvasculature. Structures are same as panel C and some are not labeled for simplicity. E. Same conditions as panels C and D, except the image is an overlay combination of panels C and D, which provides detail of conduits and microvasculature simultaneously. Structures are same as panels C and D and some are not labeled for simplicity. F. "Corkscrew" and tortuous collaterals and retrograde perfusion of superficial femoral 4 weeks after its ligation. Image captured at optimal contrast media perfusion after injection in the aorto-iliac

bifurcation. Body weight of pig is 44 kg. a-g are same as panel A, a- head of femur, hip joint, b-femur, c-gluteal artery, d-deep (profunda) femoral artery, e-superficial femoral ligation site at arrow, f-former location of superficial femoral artery, g-"corkscrew" and tortuous collaterals directly above the g, fine double arrow-retrograde perfusion (cranial direction) region of superficial femoral, h-more proximal (cranial) aspect of superficial femoral artery immediately after gluteal artery branch and above h, i-electrocardiography wires (4) extended from top middle of image to bottom right and leads at bottom middle. **Video 18.8.** Substantial retrograde perfusion at fine double arrow and perfusion in right proximal superficial femoral 4 weeks after ligation of the superficial femoral.

Figure 18.9. Renal arteries in ventrodorsal view. Body weight of pig is 40 kg. A. Right and left main renal arteries visualized by placement of guiding catheter opening in the aorta cranial to the arteries. a-vertebral column, b-tip of guidewire (curved), c-right renal artery, d-left renal artery, e-abdominal aorta, f-tip of guiding catheter. **Video 18.9.** Pulsatile perfusion of aorta and renal arteries. B. Left renal artery and fine details of renal vasculature visualized by placement of guiding catheter opening directly in the left renal artery. b, d, e, and f are same as in panel A. **Video 18.10.** Guidewire placement deep in an intrarenal artery and the clarity of renal vasculature can best be appreciated by guiding catheter placement directly in the renal artery. Contrast media is also filtered through the nephrons at the top of the kidney.

Figure 18.10. Major abdominal arteries in ventrodorsal view. Body weight of pig is 40 kg. A. Anterior mesenteric and celiac arteries. a-vertebral column, b-aorta, c-tip of guiding catheter, d-curved tip of guidewire, e-celiac artery, f-caudal edge of diaphragm, g-rib, h-cranial edge of diaphragm, i-apex of heart. j-anterior mesenteric artery. **Video 18.11.** Pulsatile perfusion of anterior mesenteric and celiac. B. Celiac artery. a-i are same as panel A. **Video 18.12.** Movement of the diaphragm and heart and pulsatile blood flow is shown in celiac and mesenteric arteries.

Figure 18.11. Forelimb and thoracic arteries in ventrodorsal view. Body weight of pig is 40 kg. A. Right forelimb. a-rib, b-heart, c-aortic arch, d-brachiocephalic trunk, e-left common carotid, f-right common carotid, g-cervical vertebrae, h-right subclavian, i-internal thoracic (mammary), j-thyrocervical, k-costocervical, l-thyrocervical trunk, m-vertebral, n-axillary, o-subscapular, p-lateral thoracic, q-brachial, r-left subclavian. **Video 18.13.** Right forelimb and thoracic arteries visualized by retrograde infusion of contrast media into right common carotid artery. B. Left forelimb. a-left subclavian, b-axillary, c-subscapular, d-brachial. **Video 18.14.** Left forelimb arteries visualized by infusion of contrast media into aortic arch.

Figure 18.12. Left carotid and cerebral arteries in ventrodorsal view. Body weight of pig is 40 kg. A. Contrast infusion into both common carotid arteries via brachiocephalic trunk. a-left common carotid, b-left internal carotid, c-rete mirabile, d-left external carotid, e-facial artery, f-masseteric branch of external carotid, g-parotid branch of external carotid, h-maxillary, i-middle meningeal (or ramus anastomosis). **Video 18.15.** Bilateral view of cerebral arteries by infusion of contrast media into brachiocephalic trunk. B. Contrast infusion into left internal carotid artery. a-c are same as panel A; ar-right common carotid, br-right internal carotid, cr-right rete mirabile, dr-right external carotid. Arrows indicate direction of contrast flow. **Video 18.16.** Significant crossover flow between the rete mirabile via the several arteries in the Circle of Willis.

Figure 18.13. Schematic of heart and major epicardial coronary arteries and interventional devices. Idealized ventrodorsal view of right coronary (RC), left anterior (ventral) descending (LAD), and circumflex (CFX) arteries. Dashed lines indicate orientation of arteries on dorsal side of the heart. Dashed rectangular object in the LAD is a coronary stent, gray rectangular object is a Transonics flow transducer, and black rectangular object in the CFX is an ameroid occluder.

Microvessels of <150 μm diameter regulate overall vascular resistance, can be seen sometimes in ideal angiography conditions, but usually their role is functionally assessed with flow velocity measures. Diagonal and obtuse marginal branches of the LAD and CFX, respectively, branch from these conduit arteries. Branches from LAD and RC that feed the ventral and dorsal aspects, respectively, of the ventricular septum are not shown.

Figure 18.14. Heart and right coronary artery in ventral views. Body weight of pig is 40 kg. A. Pure ventrodorsal view (no oblique angulation) of heart and right coronary. a-ribs, all along left and right sides of image, b-thoracic aorta, c-tip of guiding catheter at right coronary ostium, d-sinus of Valsalva (aortic valve), e-right coronary. **Video 18.17.** View of right coronary by infusion of contrast media into aortic sinus near the right coronary ostium. B. Same pure ventrodorsal view as panel A, except magnification increased. a,b-same as panel A, c-guiding catheter fully engaged in right coronary ostium, d-absence of sinus of Valsalva (aortic valve), e-proximal and distal sections of right coronary, f-fine septal branches of right coronary providing perfusion to dorsal ventricular septum. **Video 18.18.** View of right coronary by infusion of contrast media selectively into the right coronary ostium. C. Right ventral oblique 30 degrees view (Figure 18.6B) of right coronary. Spatial calibration same as panel B. a-f-same as panel A, g-sternum. **Video 18.19.** Infusion of contrast media selectively into the right coronary ostium enables visualization of right coronary and numerous septal branches. D. Left ventral oblique 30 degrees view (Figure 18.6C) of right coronary. a-g-same as panel A. **Video 18.20.** Infusion of contrast media into the right coronary ostium and spillage into the aorta enables visualization of right coronary and sinus of Valsalva (aortic valve).

Figure 18.15. Heart and left coronary arteries in ventral views. Body weight of pig is 40 kg for panels A-D, 80 kg for panels E-F. Image resolution is 300 pixels/inch for panels A-D and 91 pixels/inch for panels E-F. A. Left ventral oblique 30 degrees view (Figure 18.6C) of left coronary arteries. a-sinus of Valsalva (aortic valve) with guiding catheter near left coronary ostium, b-left anterior (ventral) descending, c-circumflex, d-obtuse marginal branch of circumflex, e-diagonal branch of left anterior descending, f-guiding catheter, g-sternum, arrowheads-small septal branches. **Video 18.21.** Infusion of contrast media into the left coronary ostium and spillage into the aorta enables visualization of left coronary arteries. B. Right ventral oblique 30 degrees view (Figure 18.6B) of left coronary arteries. Spatial calibration same as panel A. a-g and arrowheads same as panel A, h-left main. **Video 18.22.** Infusion of contrast media near the left coronary ostium yields substantial filling and visualization of the aortic valve and left coronary arteries. C. Left ventral oblique 45 degrees view of left coronary arteries. a-f and arrowheads same as panel A. **Video 18.23.** Infusion of contrast media into the left coronary ostium enables visualization of left coronary arteries, but the circumflex and obtuse marginal branches are not ideally separated. D. Right ventral oblique 45 degrees view of left coronary arteries. a-h and arrowheads same as panel B, same spatial calibration as panel C. **Video 18.24.** Infusion of contrast media near the left coronary ostium yields substantial filling and visualization of the aortic valve and best separation of circumflex and obtuse marginal branches. E. Left ventral oblique 30 degrees view of left coronary arteries in different pig than panels A-D. a-g and arrowheads same as panel A, h-extraneous wires and electrocardiogram leads. **Video 18.25.** Infusion of contrast media into the left coronary ostium enables visualization of left coronary arteries, particularly diagonal branches of left anterior descending. F. Right ventral oblique 30 degrees view of left coronary arteries. a-g and arrowheads same as panel A, h-extraneous wires and electrocardiogram leads. **Video 18.26.** Nearly selective infusion of contrast media into left coronary ostium yields best visualization of circumflex and obtuse marginal branches that are clearly separated in the right ventral oblique 30 degrees view.

Figure 18.16. Ventricular angiography and echocardiography. Left panels are obtained in control, resting conditions, right panels are during dobutamine (5 μg/kg/min) stress test. LVP-left

ventricular pressure, HR-heart rate (b/min), LV-left ventricular chamber, 2D-2-dimensional, ESV-end systolic volume, EDV-end diastolic volume. The dotted line in the angiogram in the lower right panel shows the effect of beta1 adrenergic stimulation to decrease ESV compared to resting conditions shown by the dashed line. **Video 18.27.** LV angiogram during resting conditions in adult Ossabaw pig.

Figure 18.17. 2-Dimensional and M-mode echocardiograms. Left panels are from normal, control pig; short axis view. Right two panels are from alloxan-induced diabetic dyslipidemic pig that displayed dilated cardiomyopathy and systolic dysfunction; short and long axis views are indicated. Cath-pressure catheter, PW-posterior wall, RV-right ventricular chamber, VS-ventricular septum, EDd-end diastolic dimension, ESd-end systolic dimension. Dots are separated by 1 cm and also represent the line along which the M-mode echocardiograms were obtained. Double arrows show the magnitude of the EDd and ESd. **Video 18.28.** 2-Dimensional and M-mode echocardiograms in adult Ossabaw pig.

Figure 18.18. Intravascular ultrasound (IVUS) of coronary arteries. There is one mm distance between each faint dot emanating from the center of the IVUS catheter in horizontal and vertical directions in panels A-D. Upper panels: schematic representation of angiography showing "Normal" silhouette (left), IVUS catheter (center), and IVUS image (right) (Adapted from {14233}). The angioplasty guidewire in the center panel is not shown and extends beyond the tip of the IVUS catheter more distal in the artery. A. Standard view of circumflex. a-IVUS catheter, b-guidewire artifact, c-artery lumen, d-artery wall, e-cardiac vein lumen, f-adventitia, myocardium, g-electrocardiogram. **Video 18.29.** IVUS images of circumflex during pullback of catheter over short 2 mm distance through the artery. Note especially that this video loops until stopped and, since it is such a short distance with minimal change in artery morphology, the video looks nearly stationary. B. Left anterior (ventral) descending. Structures for a-g in panel A are the same for panels B-D. h-pericardium. **Video 18.30.** IVUS images of left anterior (ventral) descending during pullback of catheter over 15 mm distance through the artery. C. Atherosclerosis of circumflex. Arrowheads indicate arc of neointimal thickening between 2 and 7 o'clock orientation. **Video 18.31.** IVUS images of circumflex during pullback of catheter over short 3 mm distance through the artery shows neointimal thickening in early stage of atherosclerosis. D. Vascular calcification of circumflex. Arrowheads indicate arc of calcification between 9 and 11 o'clock orientation. **Video 18.32.** IVUS images of circumflex during pullback of catheter through the artery shows mild intimal thickening and vascular calcification over a short 3 mm distance.

Figure 18.19. Transcutaneous femoral artery ultrasound. Electrocardiogram is shown at top. A-femoral artery, b-femoral vein, double lines show point at which pulse wave velocity was measured. **Video 18.33.** Arterial wall shows synchronous with the electrocardiogram the distensibility and the pulsatile flow velocity in the 2-D and pulse wave modes, respectively.

Figure 18.20. Coronary stent deployment in left anterior (ventral) descending coronary artery. Body weight of pigs are 44-80 kg. A. Pre-stent angiogram in left ventral oblique 30 degrees view. a-left coronary ostium, b-site of stent placement in left anterior (ventral) descending coronary artery, c-circumflex, d-obtuse marginal branch of circumflex, e-diagonal branch of left anterior descending, f-guiding catheter, g-sternum. **Video 18.34.** Pre-stent angiogram to visualize area of artery for stent deployment. B. Pre-stent intravascular ultrasound of left anterior (ventral) descending coronary artery. a-IVUS catheter, b-guidewire artifact, c-artery lumen, d-artery wall, e-adventitia, myocardium, f-electrocardiogram, g-pericardium. Arrowheads indicate arc of neointimal thickening between 4 and 8 o'clock orientation. White dots are added to clarify the one mm distance between each dot emanating from the center of the IVUS catheter in horizontal and vertical directions. **Video 18.35.** IVUS images of left anterior (ventral) descending during

pullback of catheter over 14 mm distance through the artery showing proximal diagonal branch. C. Stent deployment angiogram in left ventral oblique 30 degrees view. b-site of stent deployment is shown by balloon inflation to 1.3 times normal artery diameter. Spatial calibration is same as panel A. **Video 18.36.** Stent deployment is shown by balloon inflation in angiogram. D. Stent design and after deployment. Left-meshwork of stainless steel wire of stent is typically <1 mm in diameter (vertical double arrow) before deployment. Right-final deployment to 3.5 mm in coronary artery. E. Post-stent angiogram immediately after stent deployment. Spatial calibration and features are same as panel A. b-site of stent placement with maintained distension to 1.3 times normal artery diameter. **Video 18.37.** Successful distension of artery after stent deployment to 1.3 times normal artery diameter. F. Post-stent intravascular ultrasound immediately after stent deployment. g-pericardium. Arrowheads pointing to bright, echogenic features indicate struts of stent. **Video 18.38.** IVUS images show successful stent apposition to the arterial wall at a diameter of 4.2 mm, compared to 3.2 mm for the pre-stent control in panel B.

Figure 18.21. Post-stent stenosis of left anterior (ventral) descending coronary artery 4 weeks after stent deployment. Body weight of pigs in panels A and B are 80 and 87 kg, respectively. A. 4-week post-stent angiogram in left ventral oblique 30 degrees view. a-left coronary ostium, b-site of stent placement in left anterior (ventral) descending coronary artery with significant stenosis (arrow), c-circumflex, d-obtuse marginal branch of circumflex, e-diagonal branch of left anterior descending, f-guiding catheter. **Video 18.39.** Post-stent angiogram visualizing in-stent stenosis. B. 4-week post-stent intravascular ultrasound. There is one mm distance between each faint dot emanating from the center of the IVUS catheter in horizontal and vertical directions. a-IVUS catheter, b-guidewire artifact, c-artery lumen, d-artery wall, e-adventitia, myocardium, f-electrocardiogram, g-pericardium, h-neointima. Arrowheads pointing to bright, echogenic features indicate struts of stent. **Video 18.40.** IVUS images show neointimal hyperplasia resulting from the balloon over-inflation injury in a crescent moon-like shape medial to the echogenic arcs of the stent struts. C. Quantification of IVUS images as in panel B after coronary stenting shows Ossabaw pigs have ~4-fold greater percent stenosis than Yucatan pigs ($p<0.05$, N=6 and 8/group).

Figure 18.22. Coronary blood flow. A. Left anterior (ventral) descending coronary artery blood flow velocity at baseline and during exposure to adenosine (1 μg/kg, intracoronary). Upper panel: top trace-ECG, middle trace-aortic pressure, bottom waveform-instantaneous blood flow velocity envelopes. Lower panel: left-baseline parameters before adenosine infusion, right-peak responses to adenosine, S (and vertical line)-start of systole, D (and vertical line)-start of diastole. Leftmost panel relevant parameters: APV-average peak velocity (cm/s), DSVR-diastolic / systolic velocity ratio, BAPV-base average peak velocity (cm/s), PAPV-peak average peak velocity (cm/s), RATIO-coronary flow reserve ratio (PAPV/BAPV). **Video 18.41.** Cardiometrics FlowMap recording shows instantaneous peak blood velocity signals in real time. B. Diastolic / systolic velocity ratio (DSVR) for major epicardial conduit arteries: circumflex, left anterior (ventral) descending, and right coronary (N=6 pigs/group).

Figure 18.23. Angiograms obtained 4 weeks after placement of ameroid occluder on circumflex coronary artery. A. Left ventral oblique view. a-ameroid occluder, b circumflex artery, c-left anterior descending artery, d-septal branch of left anterior descending artery, e-ostium, f-guiding catheter. **Video 18.42.** Left ventral oblique view provides ambiguous view of source of perfusion of circumflex, but clearly shows that the septal branch is not perfusing the circumflex. B. Right ventral oblique view. Abbreviations are same as panel A; g-collateral artery. **Video 18.43.** Right ventral oblique view provides clear view of collateral artery perfusing circumflex and complete occlusion of main, native circumflex.

Figure 18.24. Superimposed positron emission tomography (PET) and computed tomography (CT) images. Coronal (upper panels A-C) and sagittal (lower panels D-F) images of a female Ossabaw pig. Panels on the left (A,D) are x-ray CT images. The righthand panels (C,F) are PET images of nitrogen-13 ammonia uptake. The center panels (B,E) are superimposed (fused) PET and CT images. a-ribs, b-liver, diaphragm, c-heart, d- nitrogen-13 ammonia uptake in ventricular wall, e- nitrogen-13 ammonia uptake in liver, diaphragm, f-vertebra, g-sternum. See also color images on CD, which display more clearly the PET images of nitrogen-13 ammonia uptake in orange color.

Figure 18.25. Positron emission tomography (PET) measurement of regional myocardial blood flow at rest (A, C) and during dobutamine stress (B, D) before (Control) and after complete circumflex coronary artery occlusion by and ameroid occluder. Arrows in C and D depict perfusion deficit as the dimmer areas. E. Myocardial regions in panels A-D perfused by the left anterior descending (LAD), circumflex (CFX), and right coronary (RC) arteries that were used to quantify perfusion in panel F. F. Plot showing relative difference in flow reserve between pig with and without ameroid occlusion of circumflex artery. Flow reserve is calculated as ratio of blood flow parameter K1 calculated from fits of compartmental models to time dependence of nitrogen-13 ammonia uptake in the myocardium. Flow reserve difference more negative than -0.15 indicates significant ischemia, most pronounced in the base and mid zones of the circumflex vascular bed.

Figure 18.26. Coronary conduit artery histology. All sections were paraffin-embedded, sectioned, and stained with Verhoeff-Van Giesen's elastin stain. A. Healthy control. a-adventitia, b-external elastic lamina, c-media, d-internal elastic lamina, intima, and endothelial cell layer, e-lumen. Inset: higher magnification of area shown by box. B. Atherosclerotic artery after 40 weeks on a high fat/high cholesterol diet that induced pronounced features of the cardiometabolic syndrome. a-e and spatial calibration are same as panel A, f-neointima. C. Yucatan in-stent stenosis. a-f are same as panel B, arrowheads-areas formerly occupied by stent struts. Inset: higher magnification of area shown by box. D. Ossabaw in-stent stenosis. a-f and arrowheads are same as panel C.

Figure 18.27. Treadmill exercise protocol for obese Ossabaw pig before and after femoral artery ligation and coronary stent placement. A. Treadmill training is done with continuous monitoring of heart rate (belt around thorax). See also color image on CD. **Video 18.44.** Early phase of exercise training protocol at moderate treadmill speed of 3 mph and 3% grade (incline). B. Heart rate (HR) response during resting, warm-up, target exercise HR, and cool-down phases of a single exercise session. C. Heart rate (HR) response in exercise training sessions during 7 weeks of chronic training. Weeks are shown for changes in the percent grade of the treadmill, stent placement, and femoral artery ligation.

Figure 18.28 Recordings of aortic pressure (top panels) and coronary blood flow (bottom panels) obtained from a conscious pig during rest and treadmill exercise as in Figure 18.27. Resting heart rate = 120; exercise heart rate = 195 b/min.
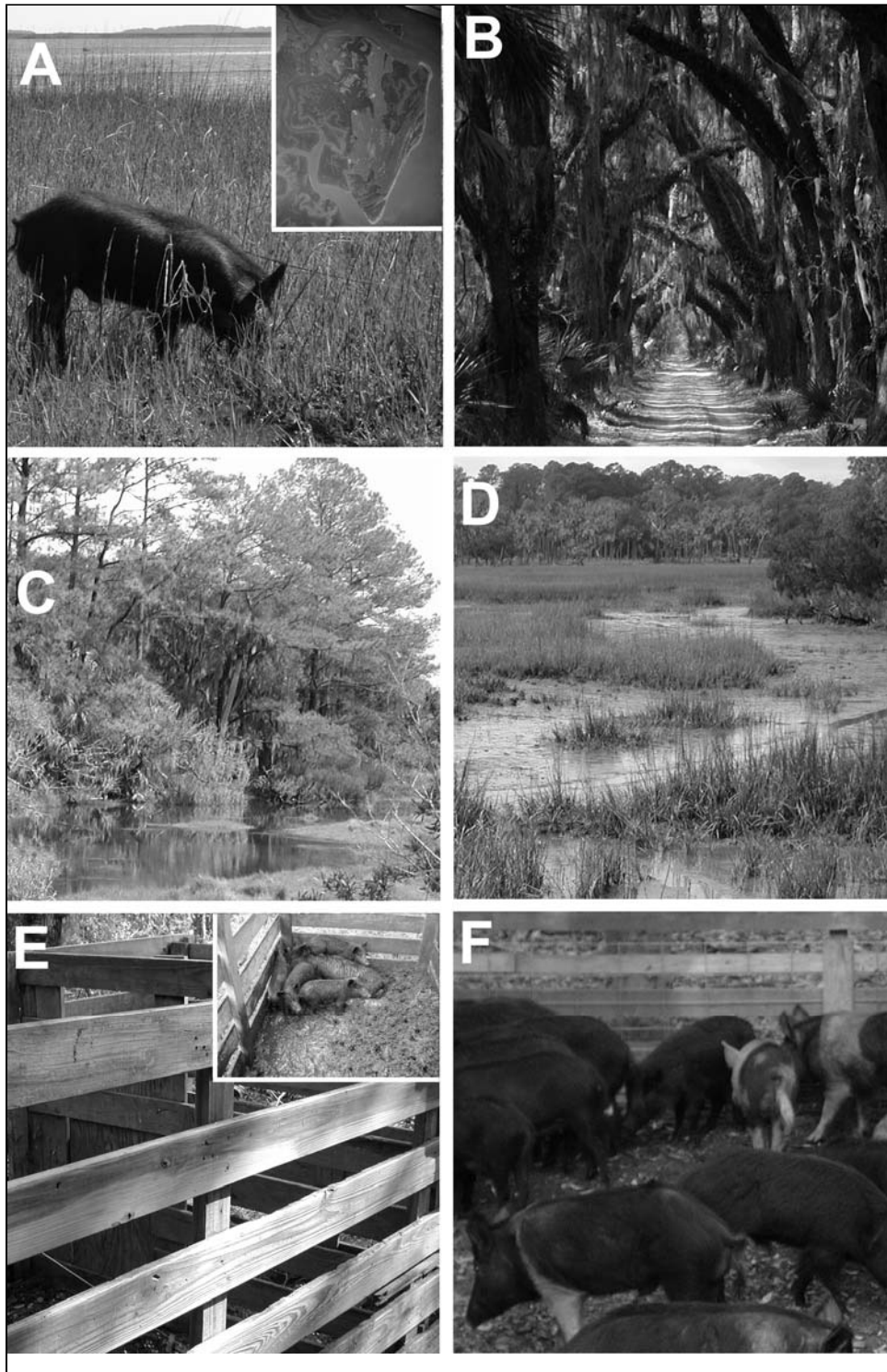
Figure 18.1

Figure 18.2

Figure 18.3
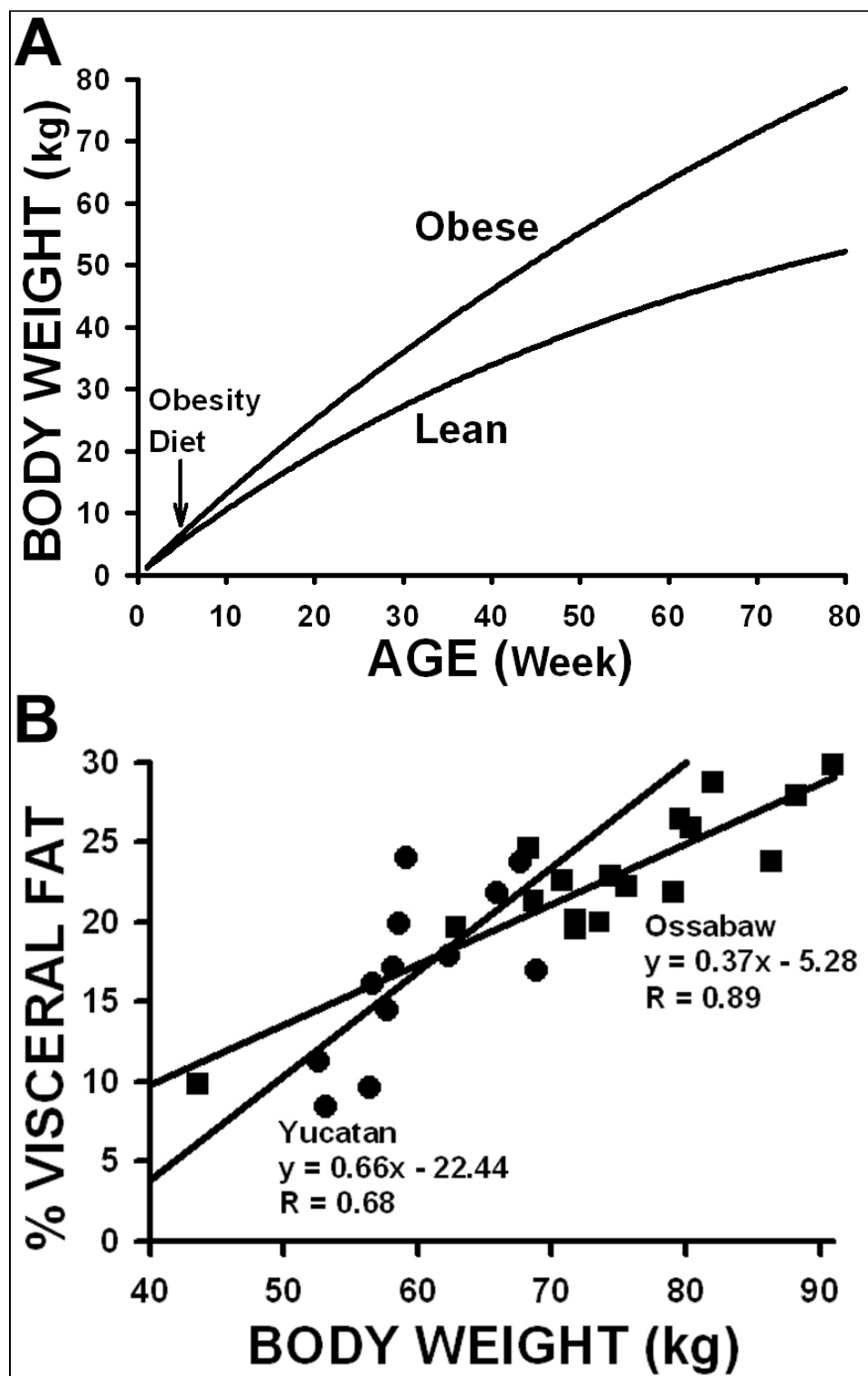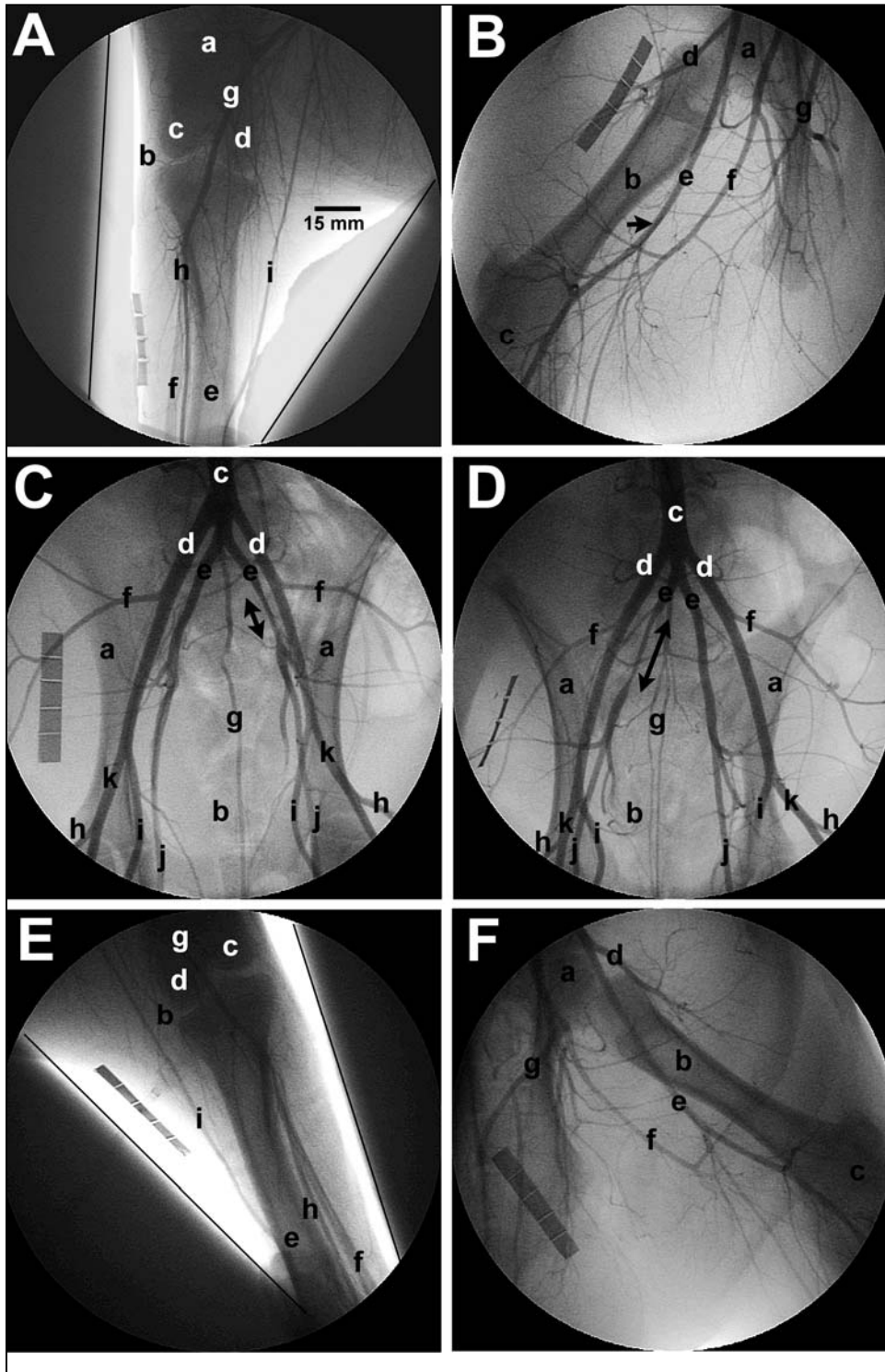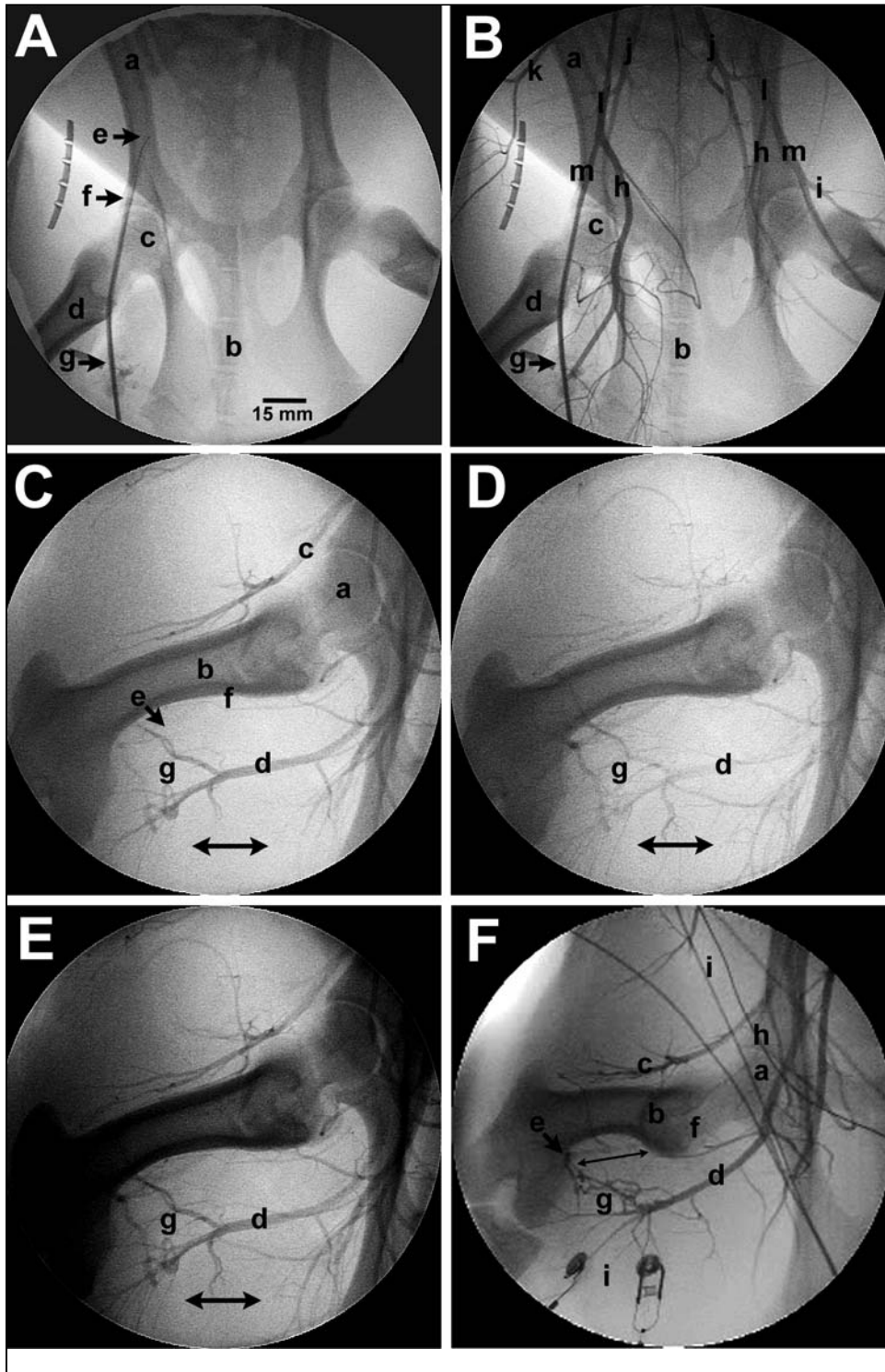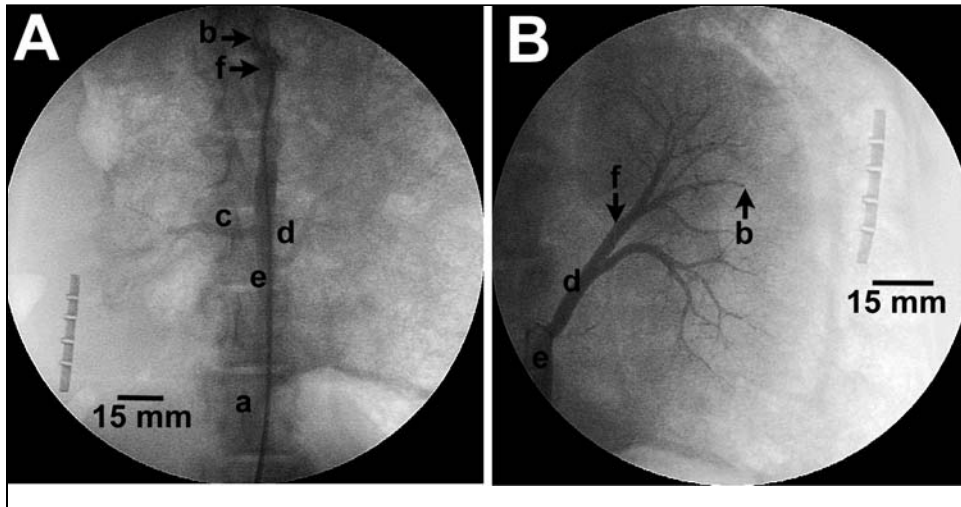
Figure 18.4
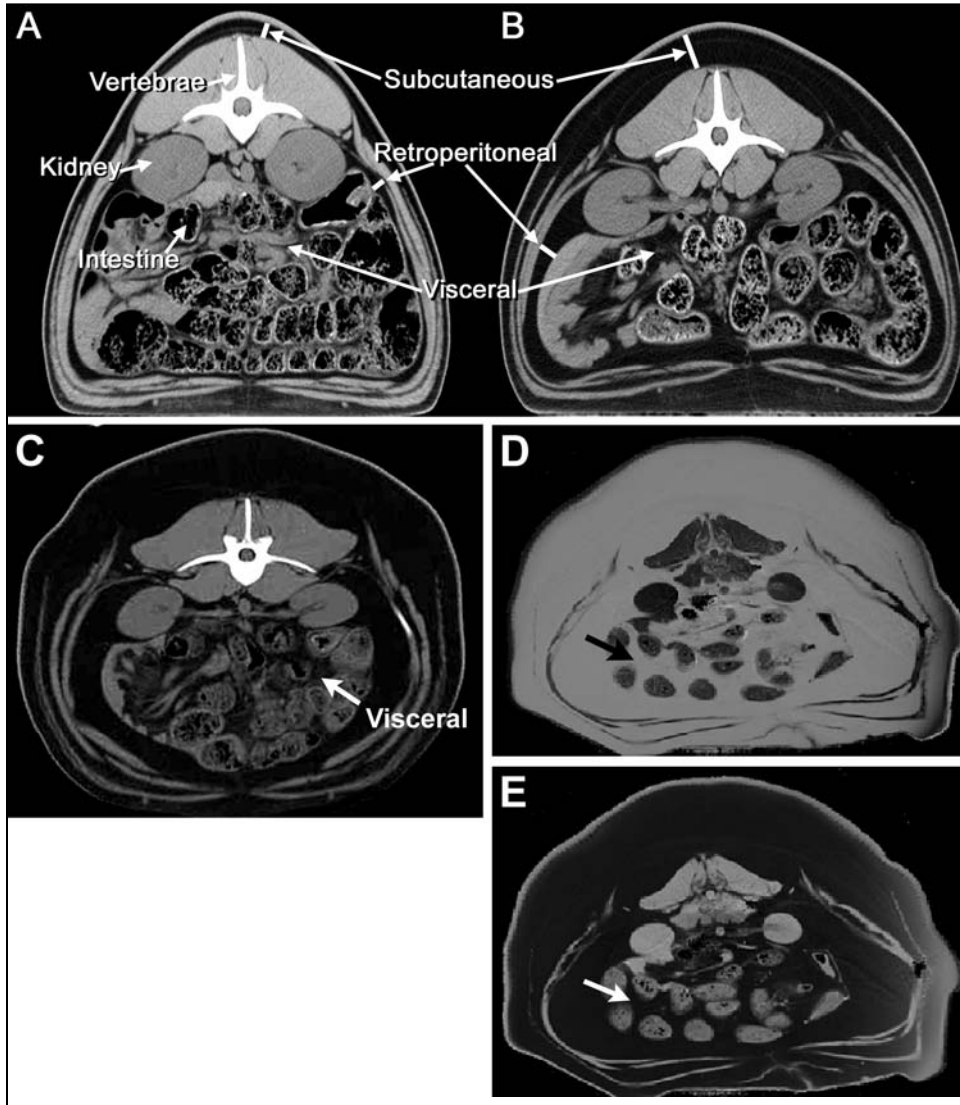
Figure 18.5
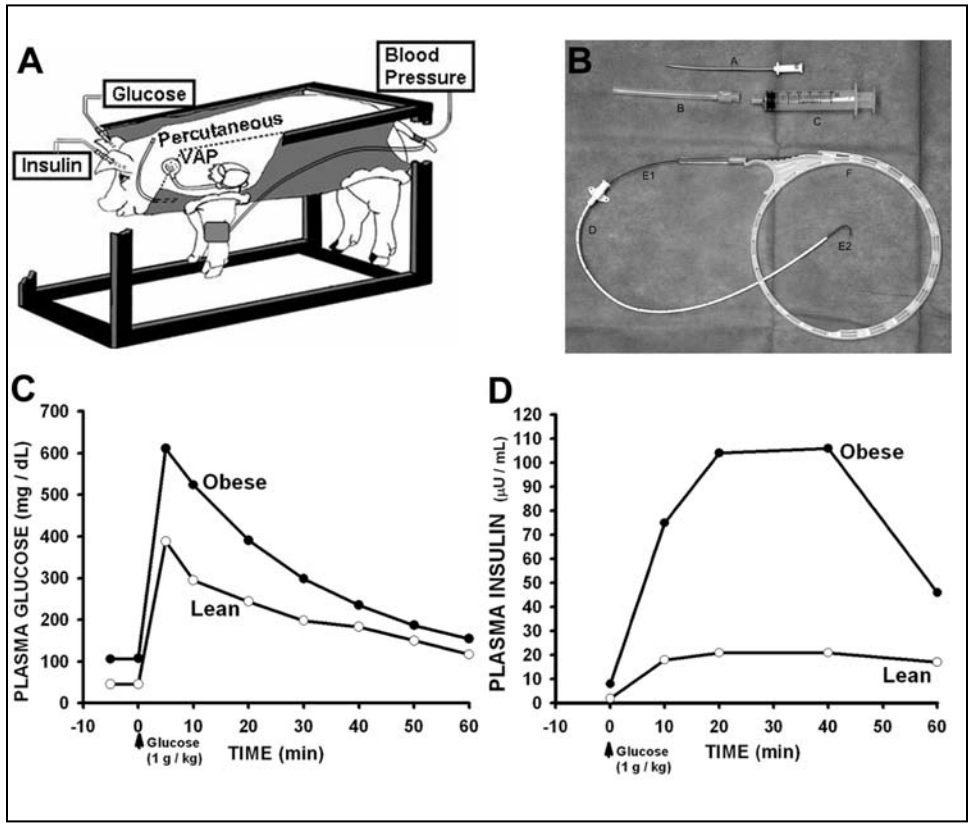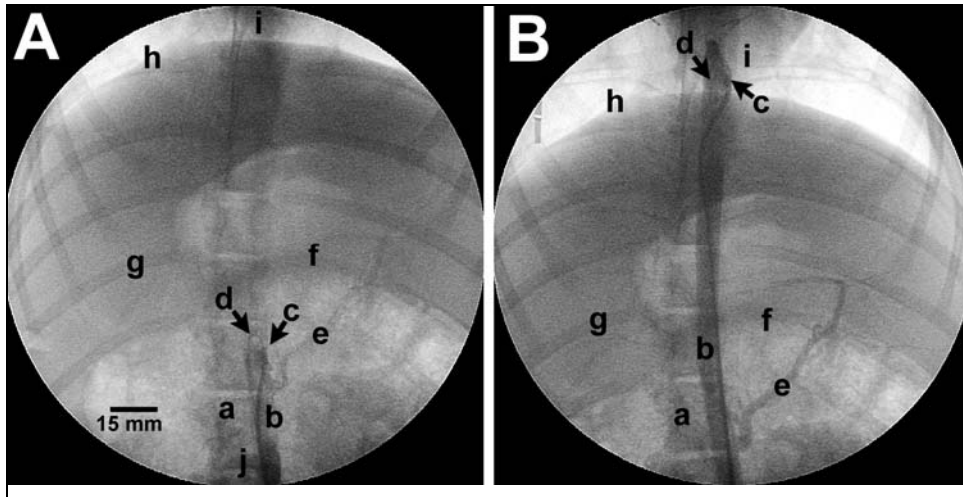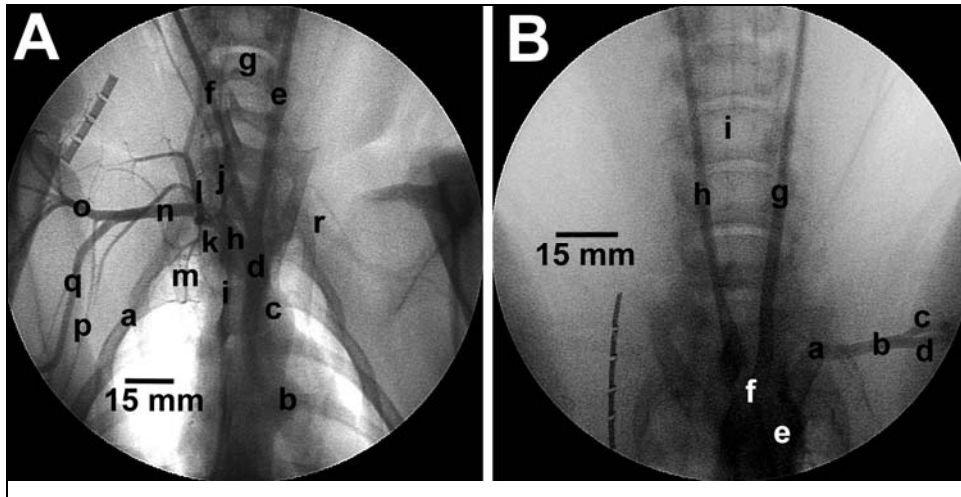
Figure 18.6
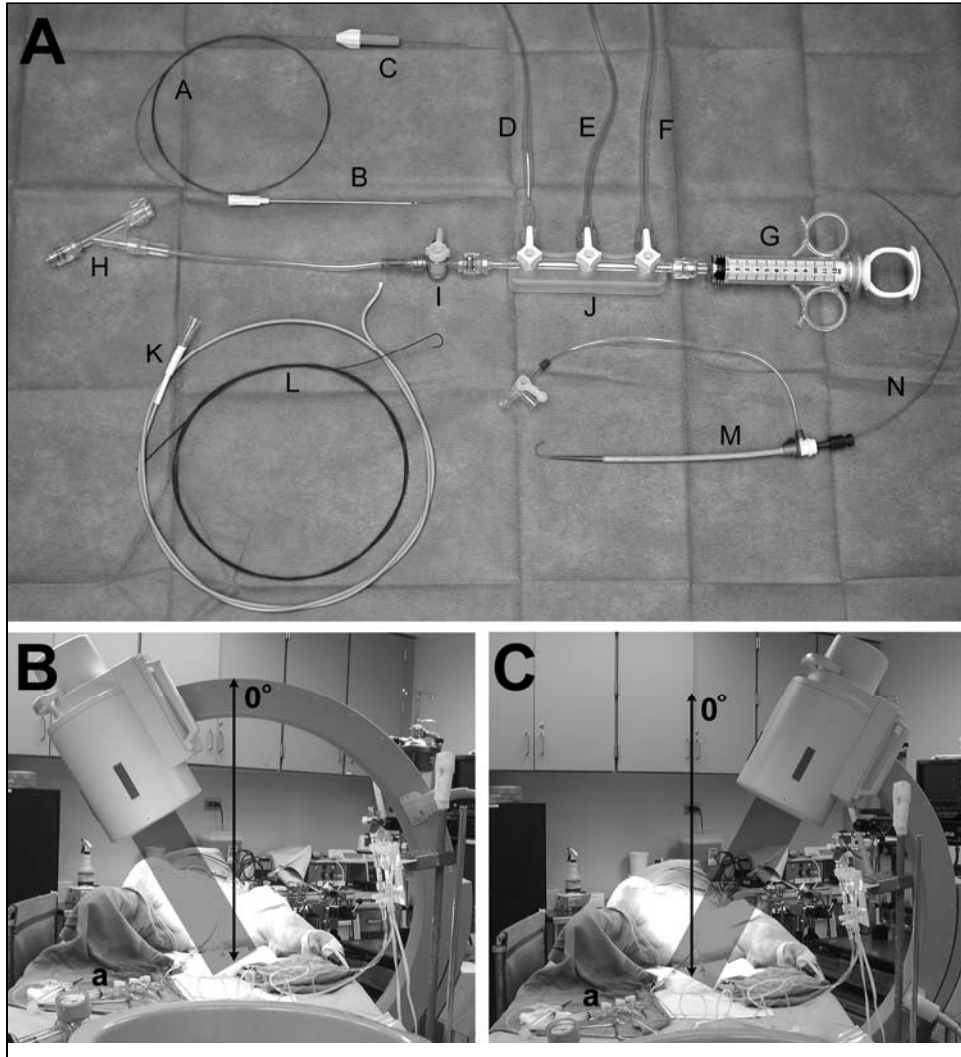
Figure 18.7

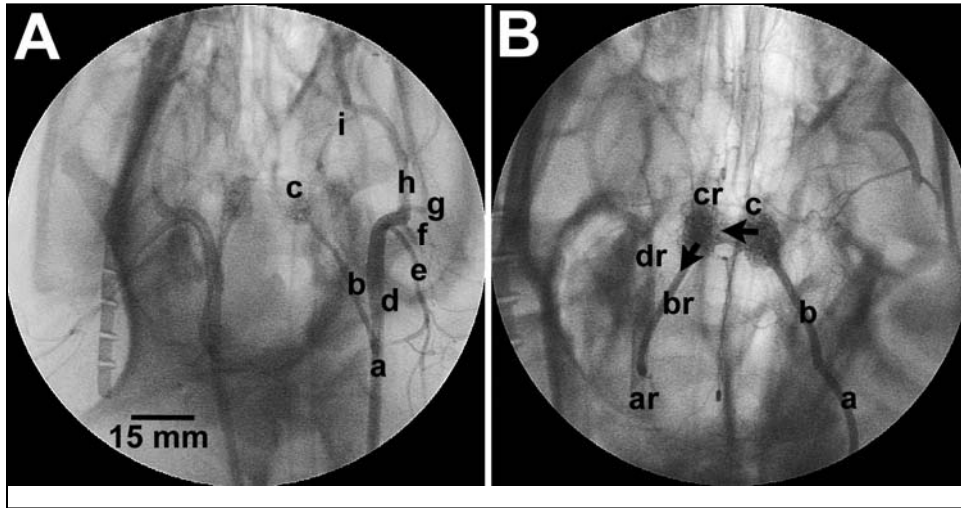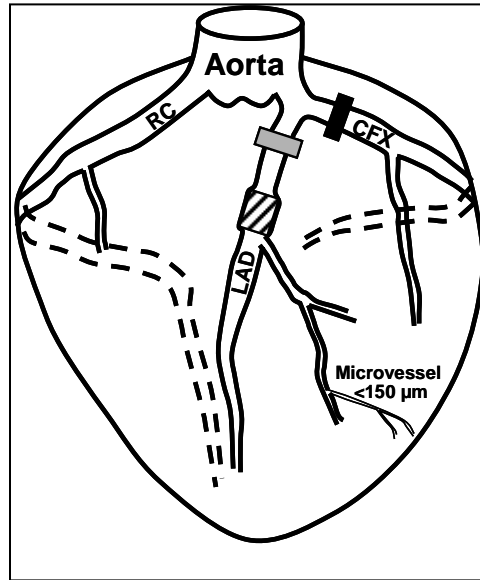Figure 18.8

Figure 18.9

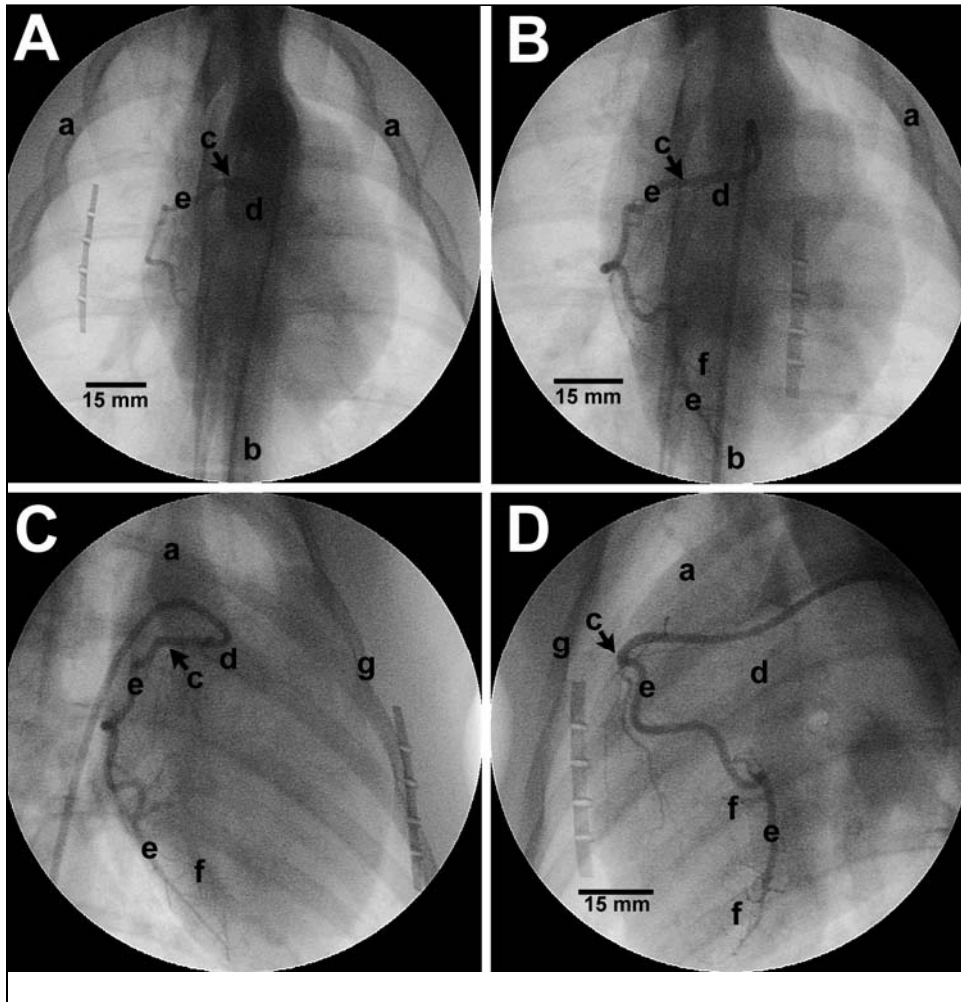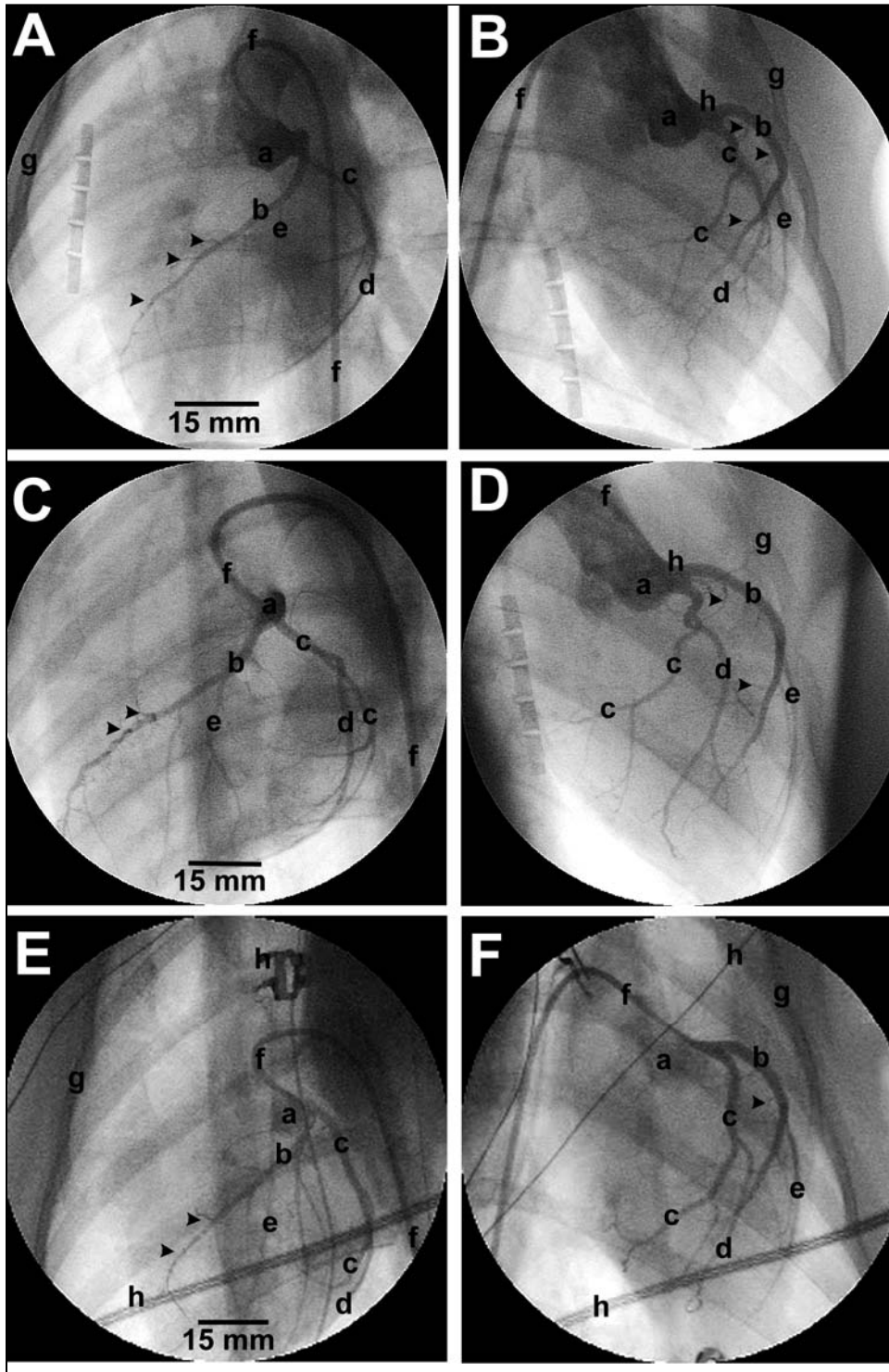Figure 18.10

Figure 18.11

Figure 18.12
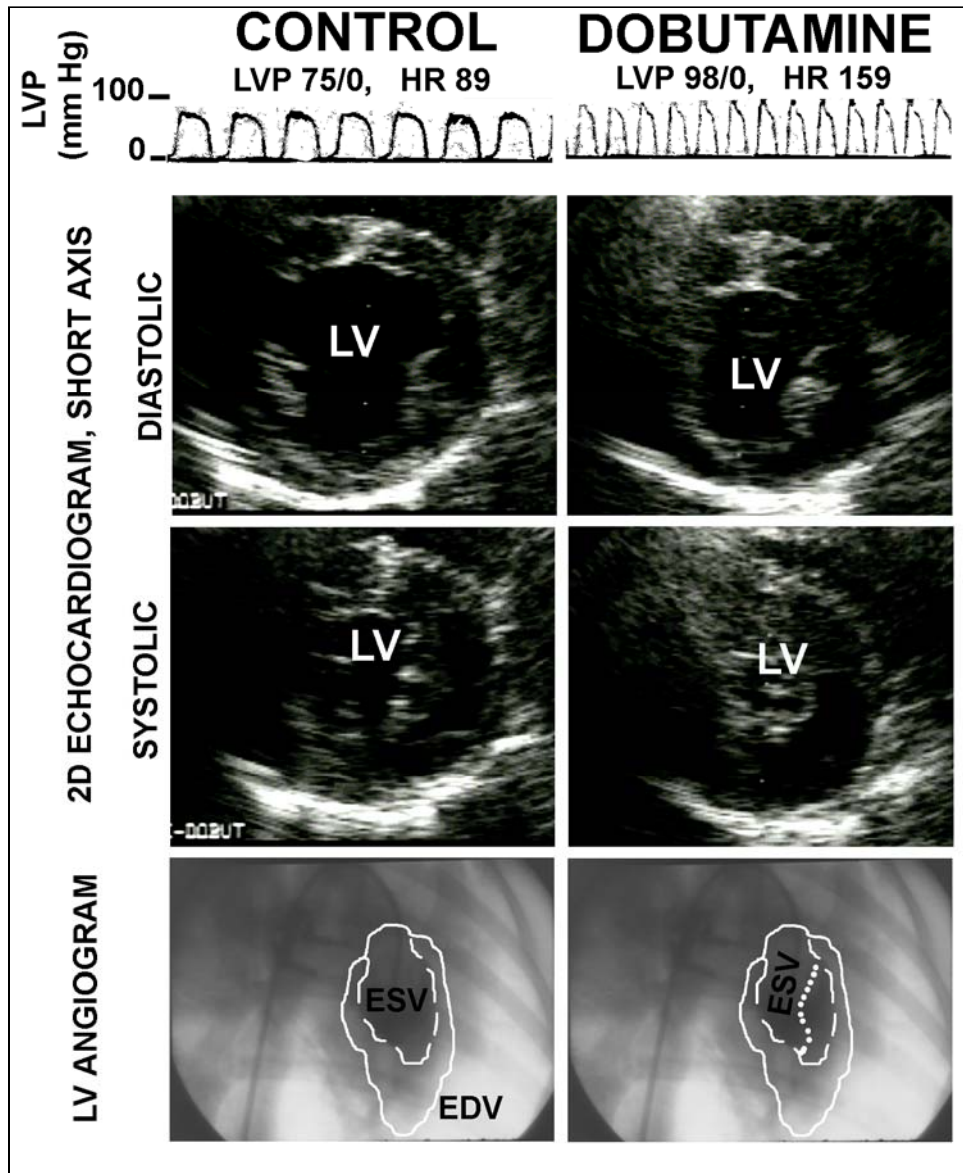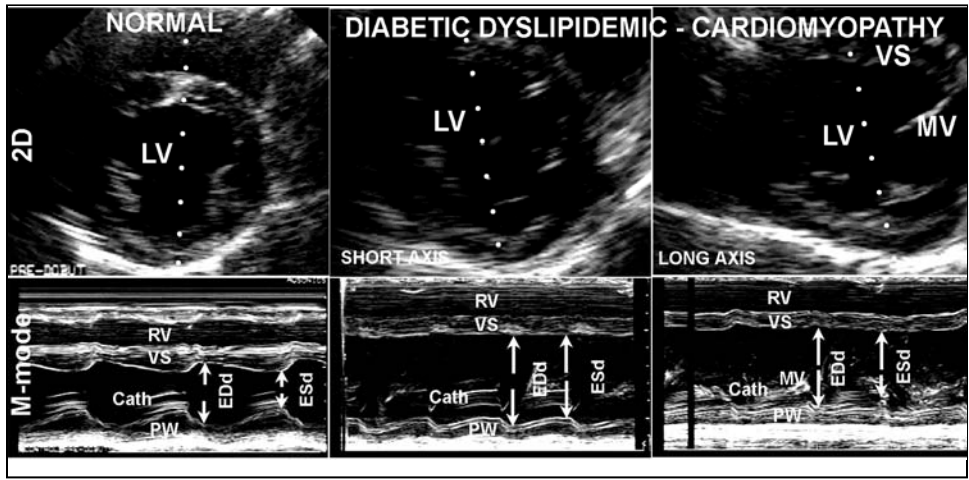
Figure 18.13

Figure 18.14
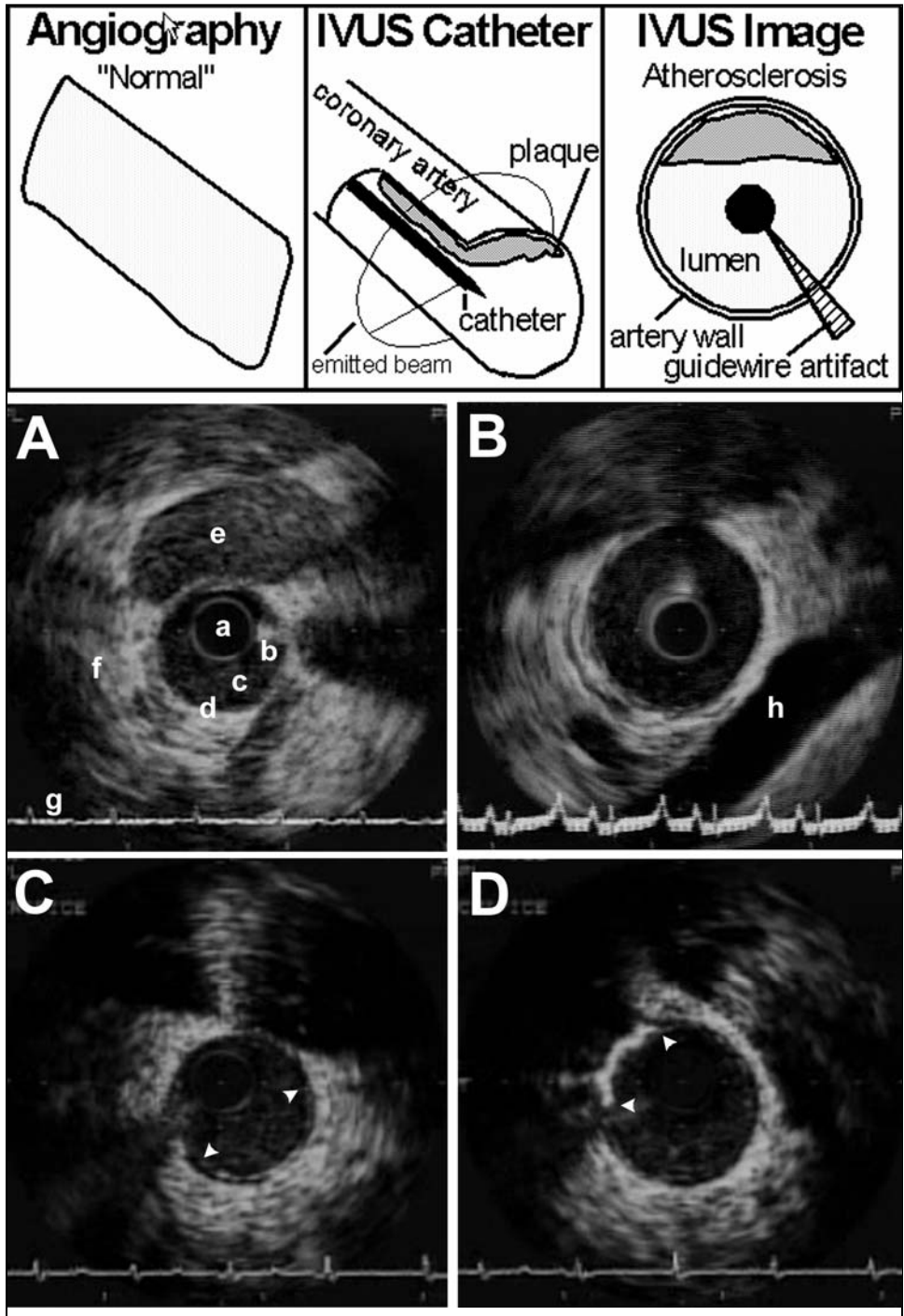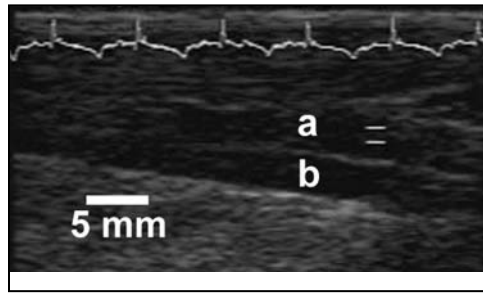
Figure 18.15

Figure 18.16
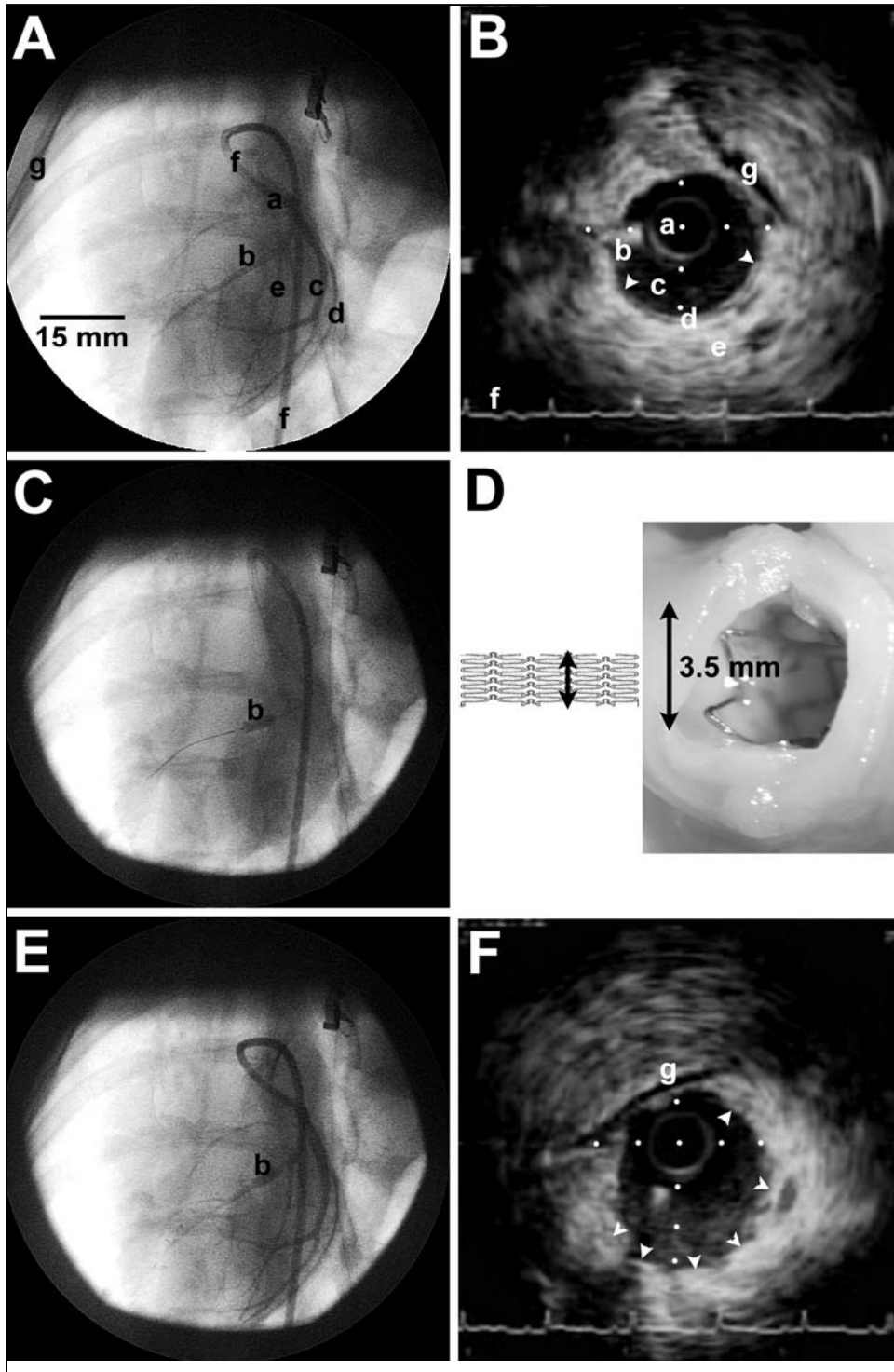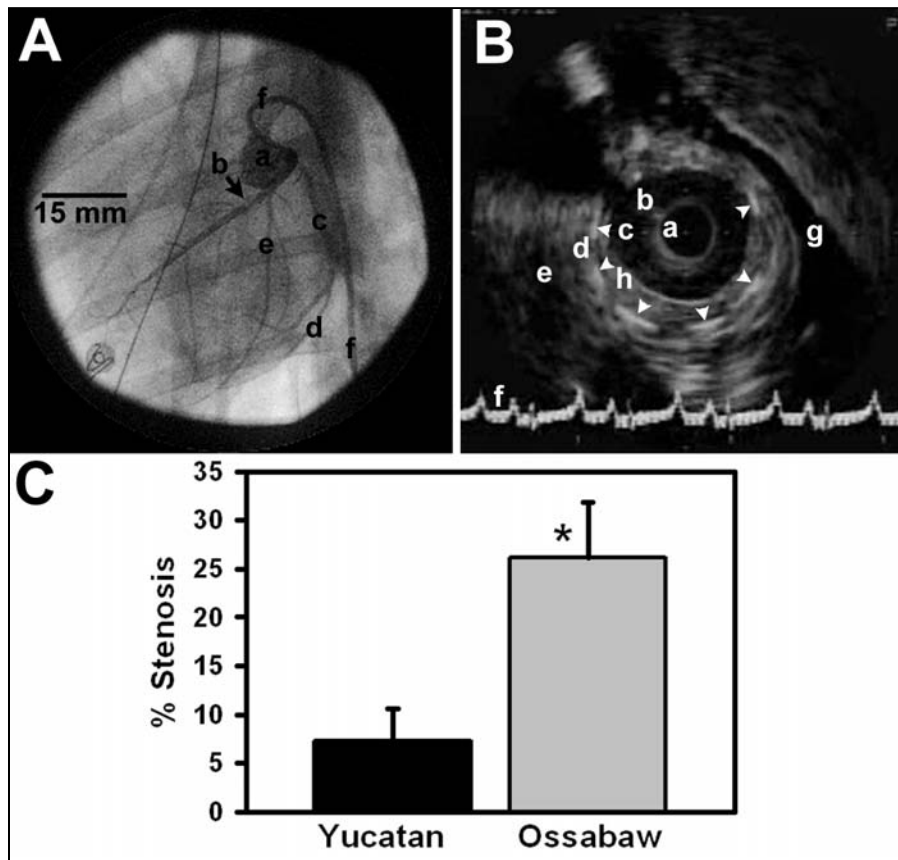
Figure 18.17

Figure 18.18

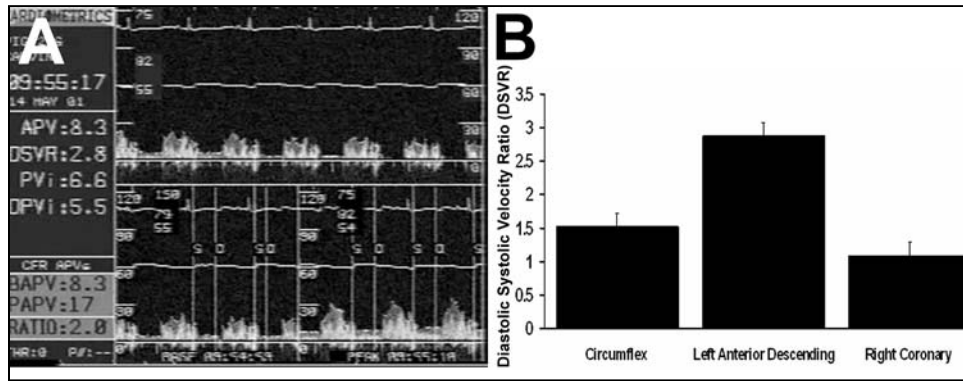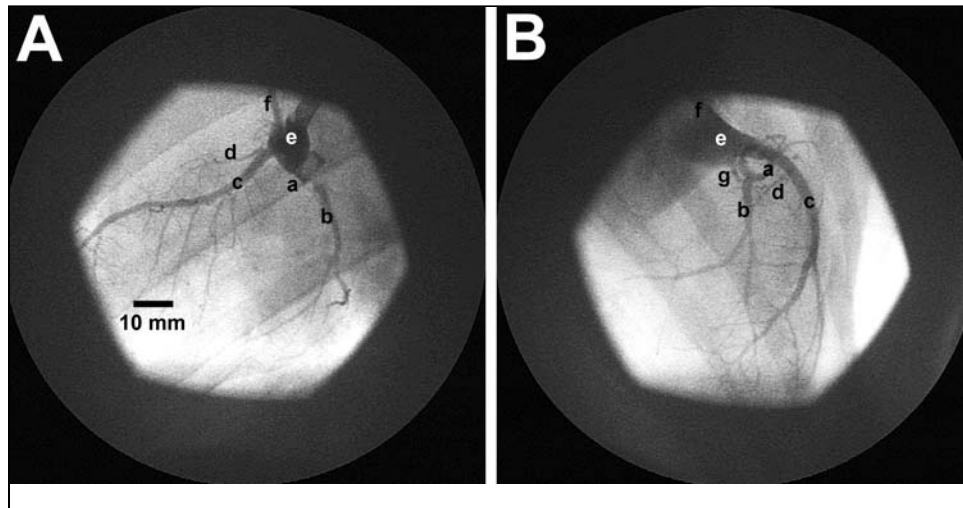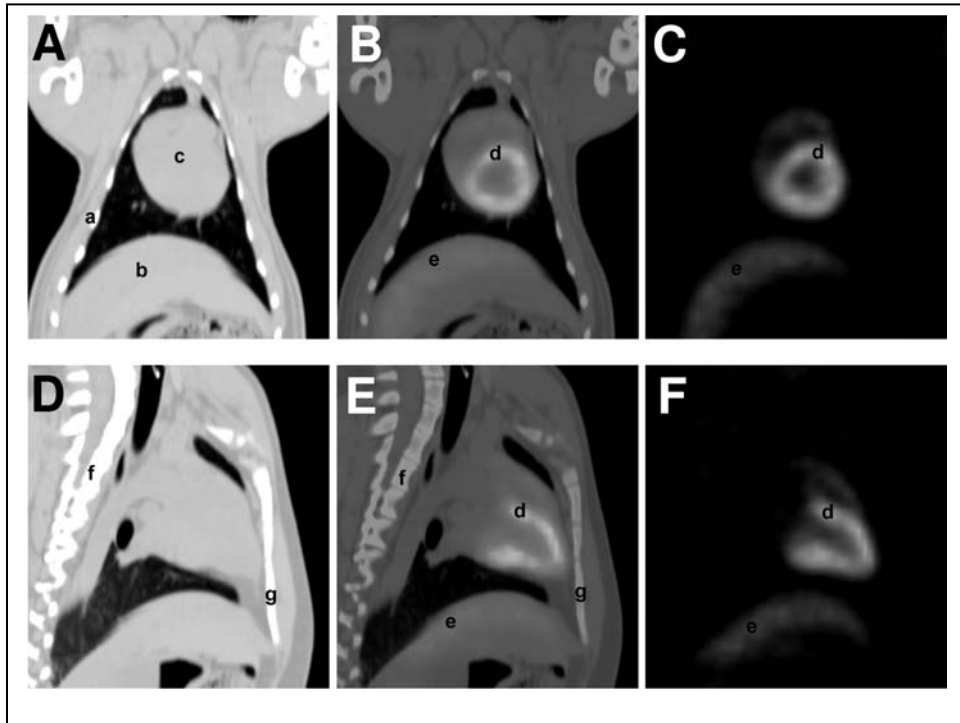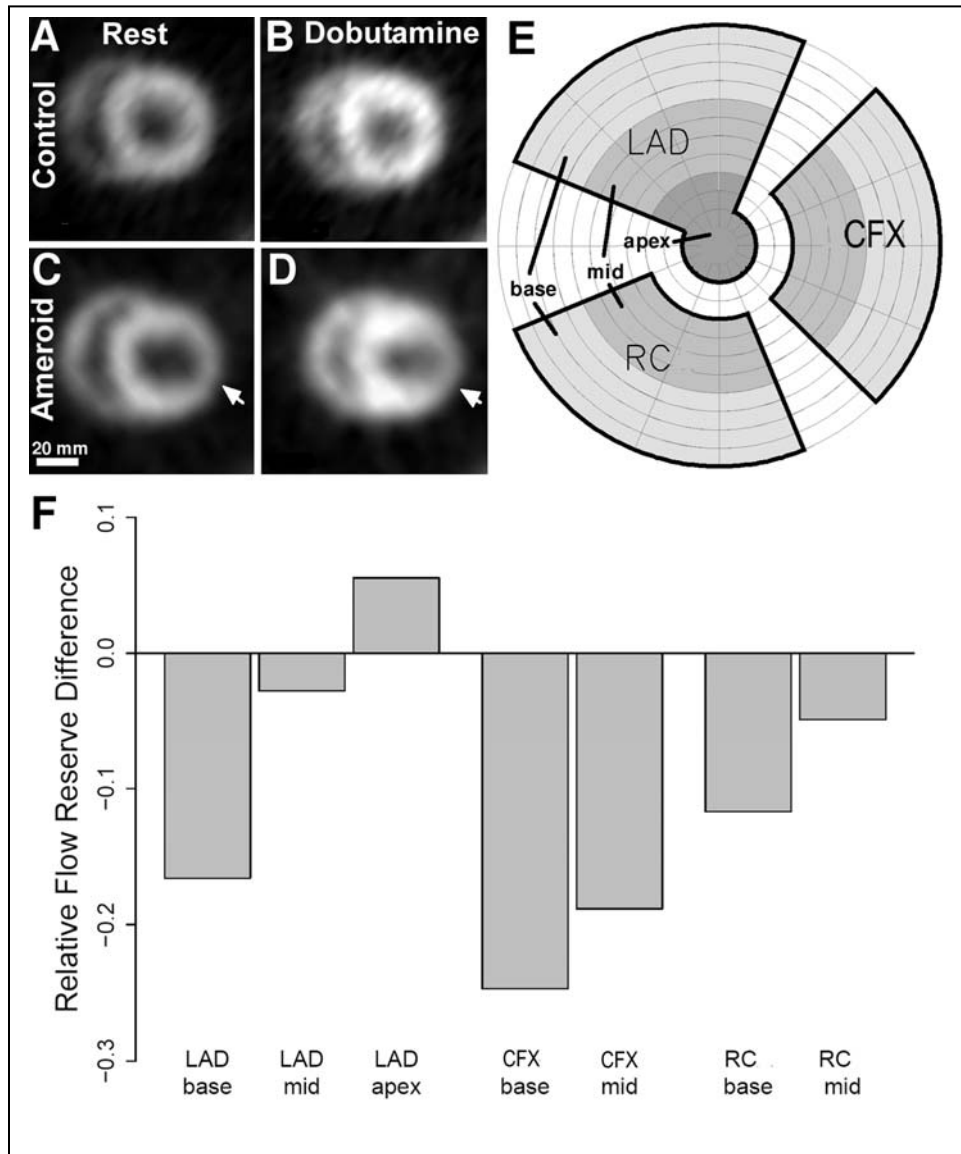Figure 18.19

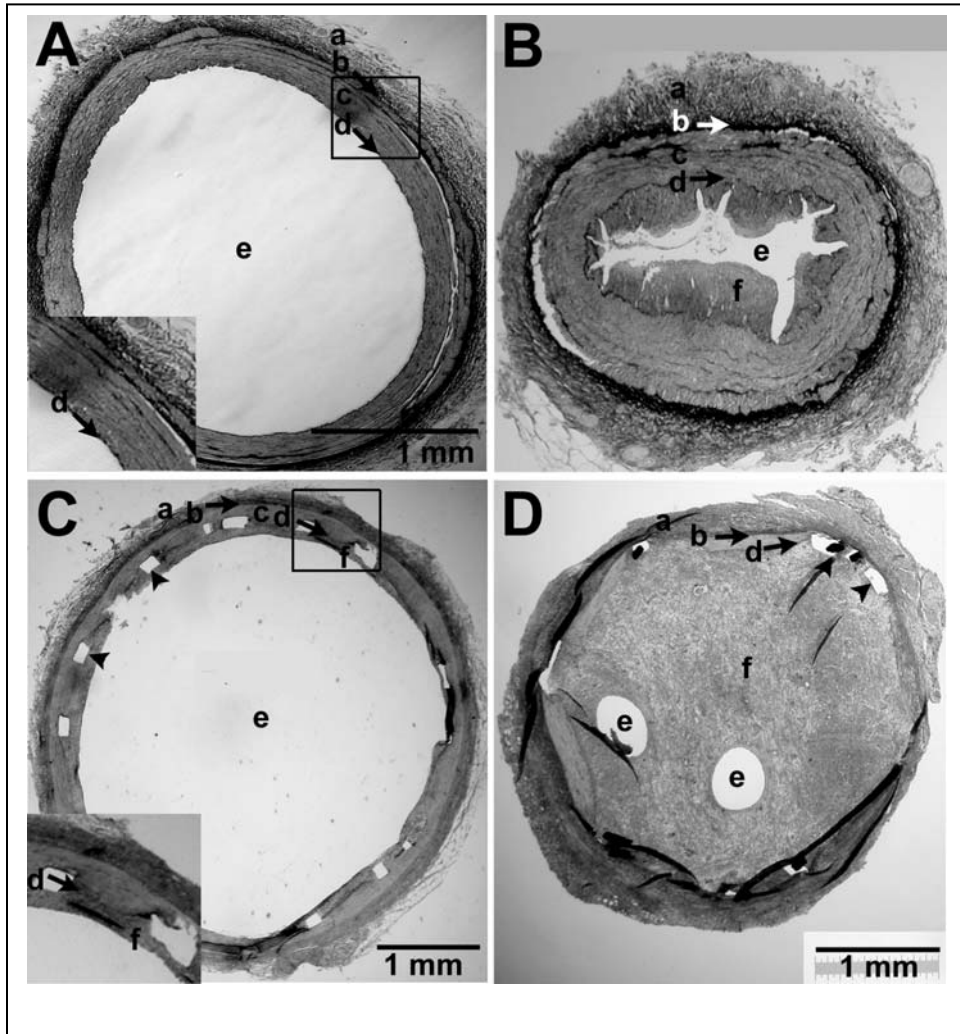Figure 18.20

Figure 18.21

Figure 18.22
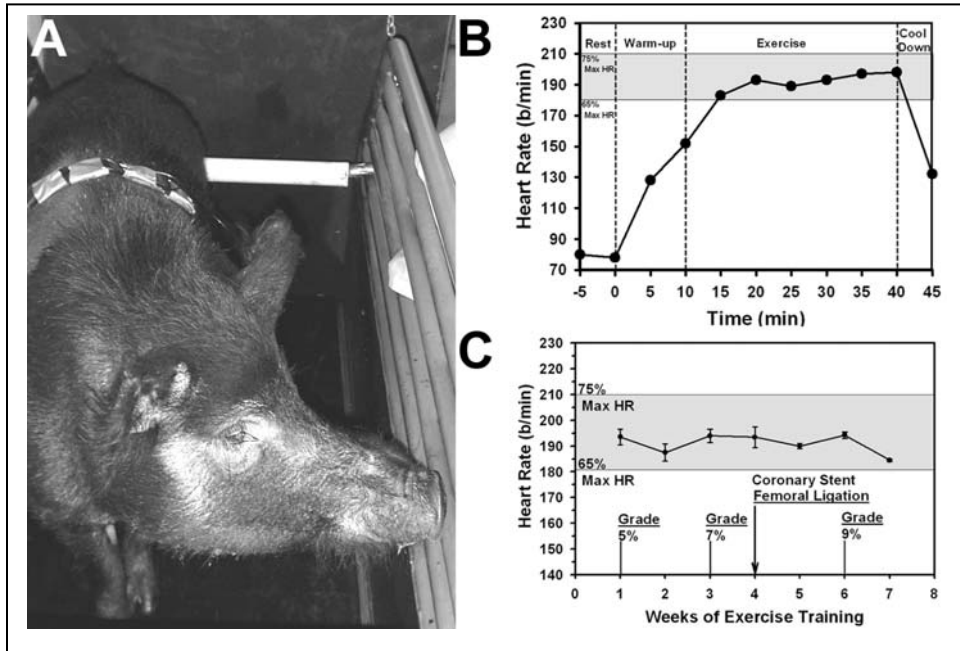
Figure 18.23

Figure 18.24

Figure 18.25

Figure 18.26

Figure 18.27

Figure 18.28